Bioorganic & Medicinal Chemistry 21 (2013) 4405–4412

Contents lists available at SciVerse ScienceDirect

Bioorganic & Medicinal Chemistry

journal homepage: www.elsevier.com/locate/bmc

Synthesis and properties of thymidines with six-membered amide bridge

Yoshiyuki Hari, Takashi Osawa, Yutaro Kotobuki, Aiko Yahara, Ajaya R. Shrestha, Satoshi Obika *

Graduate School of Pharmaceutical Sciences, Osaka University, 1-6 Yamadaoka, Suita, Osaka 565-0871, Japan

ARTICLE INFO

Article history:
Received 13 March 2013
Revised 17 April 2013
Accepted 18 April 2013
Available online 27 April 2013

Keywords:
Bridged nucleic acids
Nucleosides
Nucleotides
Oligonucleotides
Sugar modifications

ABSTRACT

Artificial thymidine monomers possessing amide or N-methylamide bridges were designed, synthesized, and introduced into oligonucleotides. UV-melting experiments showed that these oligonucleotides preferred single-stranded RNA (ssRNA) to single-stranded DNA (ssDNA) in duplex formation. Both amide- and N-methylamide-modified oligonucleotides led to a significant increase in the binding affinity to ssRNA by up to +4.7 and +3.7 °C of the T_m value per modification, respectively, compared with natural oligonucleotide. In addition, their oligonucleotides showed high stability against 3′-exonuclease.

1. Introduction

Artificial nucleic acids that possess strong and sequence-selective binding affinities with single-stranded RNA (ssRNA) and/or high nuclease-resistant properties are promising tools for nucleic acid-based technologies such as the antisense method.[1,2] In fact, a large number of nucleic acid derivatives have been developed to date.[1] The breakthrough was the discovery by us[3] and Wengel's group[4] of 2′,4′-BNA/LNA with a 2′-*O*,4′-*C*-methylene-bridged structure in the sugar moiety, (Fig. 1). The 2′,4′-BNA/LNA modification of oligonucleotides leads to a great improvement in hybridizing ability with ssRNA and an increase in nuclease resistance compared with natural oligonucleotides. Since 2′,4′-BNA/LNA was reported, the development of artificial nucleic acids with additional 2′,4′-bridged structures has attracted much attention. In particular, ring-enlargement from a five-membered bridge to a six-membered one in 2′,4′-bridged structures would be a useful modification. For example, ENA, the six-membered analog of 2′,4′-BNA/LNA, shows the same level of duplex-hybridizing ability with ssRNA as does 2′,4′-BNA/LNA, and improved enzymatic stability as compared to 2′,4′-BNA/LNA (Fig. 1).[5,6] Recently, we developed AmNA with five-membered amide bridge, the duplex-forming ability of which was comparable to that of 2′,4′-BNA/LNA, and the nuclease resistance of which was superior to that of 2′,4′-BNA/LNA.[7] Against this background, we were interested in the properties of the ring-enlarged analog of AmNA shown in Figure 2. In addition, various substituents could be introduced into the nitrogen in the amide bridge to improve the functions of the oligonucleotides. In this study, two thymidines with a six-membered amide bridge, that is, NH and NMe analogs, were synthesized, and the duplex-forming abilities and the nuclease resistances of their oligonucleotides were evaluated.

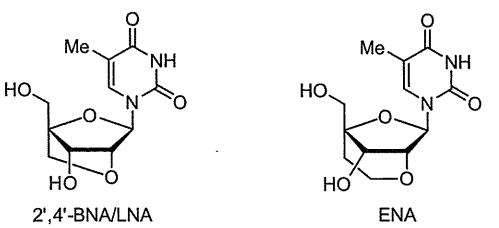

Figure 1. Structures of 2′,4′-BNA/LNA and ENA monomers.

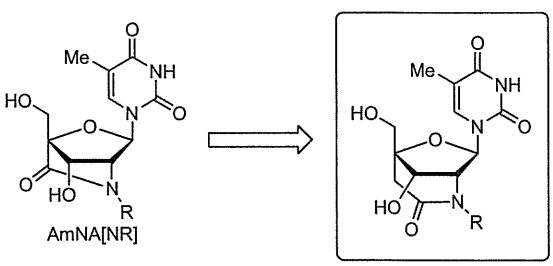

Figure 2. Design of nucleic acid monomers (R = H or Me) used in this study.

* Corresponding author. Tel.: +81 6 6879 8200; fax: +81 6 6879 8204.
E-mail address: obika@phs.osaka-ua.c.jp (S. Obika).

0968-0896/$ - see front matter © 2013 Elsevier Ltd. All rights reserved.
http://dx.doi.org/10.1016/j.bmc.2013.04.049

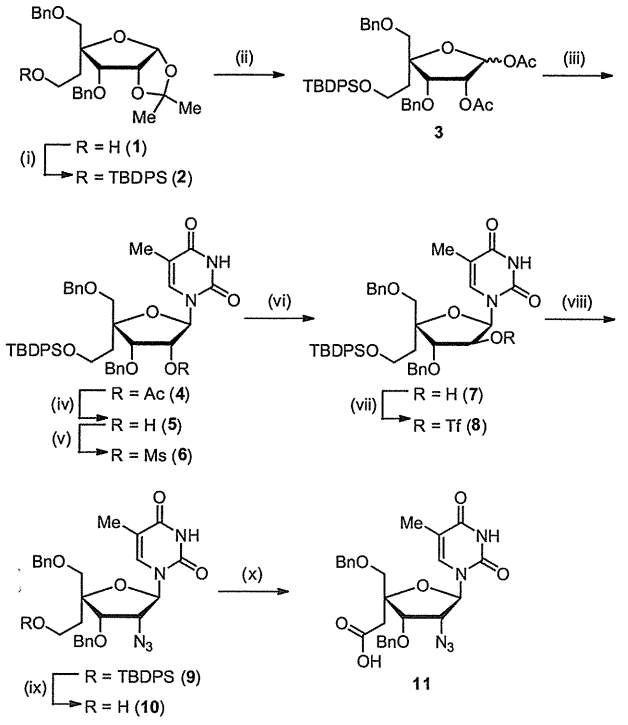

Scheme 1. Reagents and conditions: (i) TBDPSCl, DMAP, CH_2Cl_2, rt, 16 h, quant.; (ii) Ac_2O, AcOH, concd H_2SO_4, rt, 2 h, 91%; (iii) thymine, BSA, TMSOTf, MeCN, reflux, 3.5 h, 84%; (iv) K_2CO_3, MeOH, rt, 1 h, 95%; (v) MsCl, Et_3N, CH_2Cl_2, 0 °C, 1.5 h, 91%; (vi) NaOH, EtOH, rt, 12 h, 89%; (vii) Tf_2O, pyridine, CH_2Cl_2, 0 °C, 0.5 h, 83%; (viii) NaN_3, DMF, rt, 13 h, quant.; (ix) TBAF, THF, rt, 17 h, quant.; (x) PDC, MS4Å, DMF, rt, 12 h, 94%.

2. Results and discussion

2.1. Synthesis

The silylation of known compound **1**[5] using TBDPSCl gave **2** in quantitative yield (Scheme 1); **2** was converted to diacetate **3**. The reaction of **3** with silylated thymine, prepared in situ from thymine and *N,O*-bis(trimethylsilyl)acetamide (BSA), in the presence of TMSOTf produced the desired β-isomer **4**. Next, introduction of a nitrogen atom at the 2′-position was performed using a double-stereoinversion approach. After deacetylation of **4** on exposure to K_2CO_3 in MeOH, stereoinversion of the 2′-hydroxyl group was achieved by mesylation of the resulting **5**, followed by treatment with NaOH. Then, **7** underwent reaction with Tf_2O to give **8** in 83% yield, and compound **9**, with a nitrogen atom at the 2′-position, was obtained by azidation. Desilylation of **9**, followed by oxidation of **10** with PDC in DMF, efficiently produced carboxylic acid **11**.

Next, reduction of the azide group in **11** was examined (Scheme 2). Reduction by $NaBH_4$ in *i*-PrOH gave the corresponding amine **12** in 55% yield. Fortunately, under Staudinger conditions using Me_3P, ring-closed **13** was produced together with **12**. Compound **12** was converted to the desired **13** using EDC or MsCl; the yields were 72% and 86%, respectively.

The synthesis of phosphoramidite **14** was carried out in three steps from **13** (Scheme 3). Diol **15** was prepared by hydrogenolysis of **13**. Then, dimethoxytritylation of **15**, followed by phosphitylation, yielded the desired phosphoramidite **14**. Concerning the *N*-methyl congener **17**, protection of the imide nitrogen of thymine in **13**, and successive methylation of **18** gave **19**, which was hydrogenolyzed to produce diol **20**. Using a similar synthetic route to **14**, **20** was converted into the desired phosphoramidite **17** with an N-methylamide bridge via dimethoxytritylated **21**. The phosphoramidites **14** and **17** obtained were used to synthesize modified oligonucleotides **22–29** on an automated DNA synthesizer (see the Section 4 for details). These amide bridges were stable under conventional conditions, that is, aqueous ammonia or methanolic K_2CO_3, for cleavage from the resin and removal of β-cyanoethyl groups on the phosphates.

The duplex-forming abilities of oligonucleotides **22–27** with ssDNA or ssRNA were evaluated and the results are summarized in Table 1. Regardless of whether it was the NH or NMe analog, the modified oligonucleotides generally showed a significantly decreased affinity for ssDNA compared with natural oligonucleotide **30**, although in the case of **24**, possessing three NH analogs, the affinity was increased by +1.7 °C per modification. Concerning ssRNA, the single-modified oligonucleotides **22** and **25** had almost the same affinities as natural oligonucleotide **30**. However, by multiple modifications, the binding affinity was greatly increased and the changes in T_m value per modification (ΔT_m/mod.) of the NH (**24**) or NMe (**27**) analogs were +4.7 and +3.7 °C, respectively. These results demonstrate that oligonucleotides containing these thymidines with six-membered amide bridges formed stable duplexes with ssRNA and recognized ssRNA more selectively than ssDNA in the duplex formation.

The binding affinities with ssDNA and ssRNA of the oligonucleotides modified by AmNA[NH] or AmNA[NMe] with a five-membered amide bridge, shown in Figure 2, and those of the oligonucleotides modified by HxNA[NMe] with a six-membered hydroxamate bridge, shown in Figure 3, were evaluated in our previous reports.[7,8] Although these analogs showed lower duplex-forming abilities with ssRNA than AmNA[NH] or AmNA[NMe], one of these analogs, the NH analog, was more stably bound to ssRNA compared with HxNA[NMe] with a six-membered bridge similar to these amide bridges.

The stabilities of oligonucleotides **28** and **29** including these analogs against 3′-exonuclease were determined and compared with those of AmNA[NH]-, AmNA[NMe]-, and HxNA[NMe]-modified oligonucleotides **31-33** and natural **30** (Fig. 4 and the sequences of oligonucleotides used are shown in the legend of Fig. 4). Under conditions where natural **30** decomposed completely within 5 min, over 50% and 60% of **28** and **29** remained after 40 min. The NMe analog (**29**) showed higher stability against nuclease than the NH analog (**28**) did. This is probably because ac-

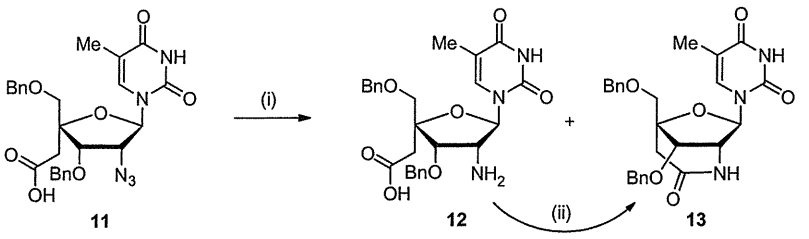

Scheme 2. Reagents and conditions: (i) $NaBH_4$, *i*-PrOH, reflux, 1 h, 55% (**12**) or Me_3P, THF/H_2O (5:1), rt, 14 h, ca 35% (**12**) and 43% (**13**); (ii) EDC, DMAP, CH_2Cl_2, rt, 24 h, 72% or MsCl, Et_3N, CH_2Cl_2, 0 °C to rt, 17 h, 86%.

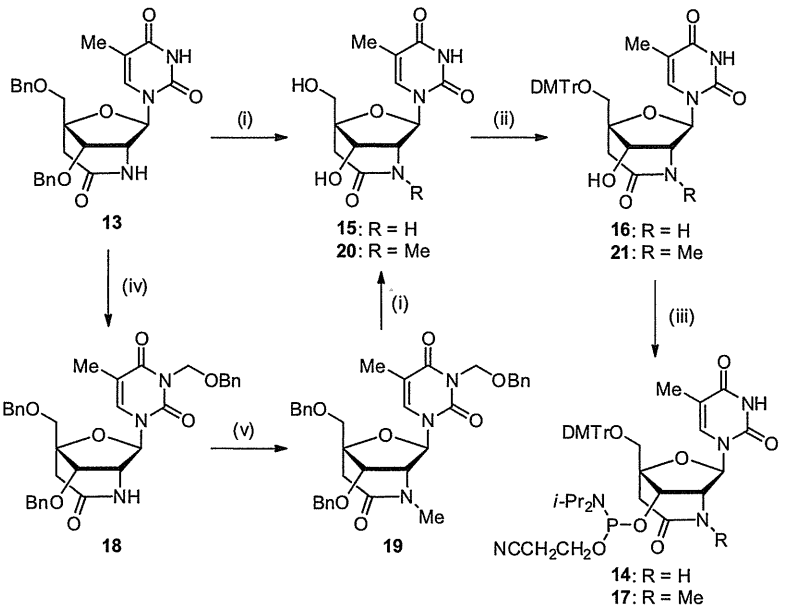

Scheme 3. Reagents and conditions: (i) H_2, 20% $Pd(OH)_2$-C, MeOH, rt, 24 h, 61% (**15**) or 20% $Pd(OH)_2$-C, cyclohexene, EtOH, reflux, 2 h, quant. (**20**); (ii) DMTrCl, pyridine, rt, 3–17 h, 81% (**16**) and 69% (**21**); (iii) $(i\text{-}Pr_2N)_2POCH_2CH_2CN$, 1*H*-tetrazole, MeCN/THF (3:1), rt, 12 h, 42% (**14**) or $i\text{-}Pr_2NP(Cl)OCH_2CH_2CN$, $i\text{-}Pr_2NEt$, CH_2Cl_2, rt, 2 h, 73% (**17**); (iv) $BnOCH_2Cl$, DBU, DMF, 0 °C, 0.5 h, 86%; (v) NaH, MeI, DMF, 0 °C, 2 h, 60%.

Table 1
T_m values (°C) of duplexes formed between oligonucleotides and ssDNA or ssRNA[a,b]

Oligonucleotide	ssDNA	ssRNA
5′-TTTTTTTTTT-3′ (**30**)	21	19
5′-TTTTTTTTTT-3′ (**22**)	16 (−5.0)	20 (+1.0)
5′-TTTTTTTTTT-3′ (**23**)	19 (−1.0)	27 (+4.0)
5′-TTTTTTTTTT-3′ (**24**)	26 (+1.7)	33 (+4.7)
5′-TTTTTTTTTT-3′ (**25**)	15 (−6.0)	20 (+1.0)
5′-TTTTTTTTTT-3′ (**26**)	13 (−4.0)	26 (+3.5)
5′-TTTTTTTTTT-3′ (**27**)	18 (−1.0)	30 (+3.7)

[a] Conditions: 10 mM sodium phosphate buffer (pH 7.2) and 100 mM NaCl. The final concentration of each oligonucleotide used was 4 μM. The sequences of ssDNA and ssRNA are 5′-d(AAAAAAAAAA)-3′ and 5′-r(AAAAAAAAAA)-3′, respectively. *T* and T indicate NH analog and NMe analog, respectively.

[b] The change in T_m value per modification is shown in parentheses.

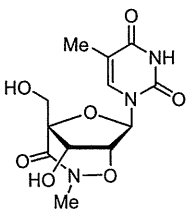

Figure 3. Structure of HxNA[NMe] monomer.

cess of the nuclease to the phosphodiester linkage was prevented by the more bulky N-methylamide bridge. In a comparison of **28** and **29** with **31** and **32**, respectively, no significant improvement in nuclease resistance as a result of enlargement of the amide bridge was observed. However, oligonucleotides **28** and **29** were quite stable compared with **33**, including an HxNA[NMe] with the same six-membered ring size. In contrast, the six-membered hydroxamate bridge of HxNA was opened under the nuclease treatment conditions, and, consequently, the 5′-phosphate moiety of HxNA showed high resistance against nuclease.[8] However, in the

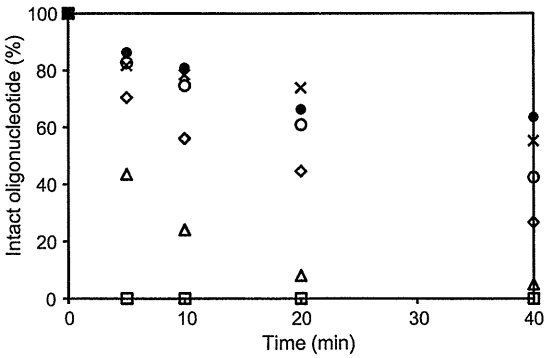

Figure 4. Enzymatic stability of oligonucleotides **28** and **29**. Conditions: 1.75 μg/mL Crotalus admanteus venom phosphodiesterase (CAVP), 10 mM $MgCl_2$, 50 mM Tris-HCl (pH 8.0), and 7.5 μM each oligonucleotide at 37 °C. The sequence of oligonucleotides used was 5′-TTTTTTTTTT-3′. T = NH analog (open circle, oligonucleotide **28**), NMe analog (closed circle, oligonucleotide **29**), AmNA[NH] (open diamond, oligonucleotide **31**), AmNA[NMe] (cross, oligonucleotide **32**), HxNA[NMe] (open triangle, oligonucleotide **33**) and natural (open square, oligonucleotide **30**).

cases of these NMe and NH analogs bearing a six-membered amide bridge, as well as AmNA[NH] and AmNA[NMe] bearing a five-membered amide bridge, the 5′-phosphate moieties were easily degradable and such a phenomenon was not observed. These results suggest that resistance against nuclease was greatly affected by not only the bridge size but also by the composition of the bridge, for example, whether there is any substituent and/or heteroatom, or the location of the substituent and/or heteroatom.

3. Conclusion

Two thymidines bearing six-membered bridges, that is, amide and N-methylamide bridges, were successfully synthesized and introduced into oligonucleotides, using an automated DNA synthesizer. These oligonucleotides formed stable duplexes with ssRNA, but the duplexes with ssDNA were destabilized. They also had high nuclease resistance, which were slightly better than those of

AmNAs bearing five-membered amide bridges. Moreover, their nuclease resistances were much higher than that of HxNA[NMe] with the same bridge size. These findings demonstrated that the composition of the bridge moiety is a key factor in the development of bridged nucleic acids. We believe that the accumulation of properties such as duplex-forming ability and nuclease resistance through the development of various bridged nucleic acids will contribute to developing ideal useful tools for nucleic acid-based technologies.

4. Experimental

4.1. General

All chemicals were purchased from chemical suppliers. For column chromatography, Fuji Silysia silica gel PSQ-100B and FL-100D were used. All melting points were measured on a Yanagimoto micro melting point apparatus and are uncorrected. ^{1}H NMR, ^{13}C NMR and ^{31}P NMR spectra were recorded on a JEOL ECS400 spectrometer. IR spectra were recorded on JASCO FT/IR-200 and JASCO FT/IR-4200 spectrometers. Optical rotations were recorded on a JASCO DIP-370 instrument. Mass spectra were measured on a JEOL JMS-600 or JEOL JMS-700 mass spectrometer. MALDI-TOF mass spectra were recorded on a Bruker Daltonics Autoflex II TOF/TOF mass spectrometer.

4.2. 3,5-Di-*O*-benzyl-4-(2-*tert*-butyldiphenylsiloxyethyl)-1,2-*O*-isopropylidene-α-D-ribofuranose (2)

Under nitrogen atmosphere, DMAP (350 mg, 2.87 mmol), Et_3N (4.0 mL, 29 mmol), and TBDPSCl (4.0 mL, 15 mmol) were added to a solution of alcohol **1**[5] (3.96 g, 9.56 mmol) in CH_2Cl_2 (100 mL) at 0 °C. The reaction mixture was stirred at room temperature for 16 h. The reaction was then quenched with satd $NaHCO_3$ aq and extracted with CH_2Cl_2 (3 × 100 mL). The combined organic layer was washed with water and brine, dried over Na_2SO_4, and concentrated. The obtained crude residue (8.82 g) was purified by column chromatography (silica gel 200 g, *n*-hexane/EtOAc = 10:1) to give silyl ether **2** (6.28 g, quant.) as a colorless oil.

$[\alpha]_D^{25}$ +16.3 (*c* 1.00, $CHCl_3$). IR (KBr): 3068, 3031, 2932, 2857, 1496, 1472, 1454, 1428, 1383, 1312, 1256, 1209 cm^{-1}. ^{1}H NMR (400 MHz, $CDCl_3$): δ 1.00 (s, 9H), 1.30 (s, 3H), 1.50 (s, 3H), 1.87 (ddd, *J* = 7.0, 8.0, 14.5 Hz, 1H), 2.43 (ddd, *J* = 5.0, 6.5, 14.5 Hz, 1H), 3.29 (d, *J* = 10.5 Hz), 1H, 3.70 (d, *J* = 10.5 Hz, 1H), 3.82 (ddd, *J* = 5.0, 7.0, 12.0 Hz, 1H), 3.94 (ddd, *J* = 6.5, 8.0, 12.0 Hz, 1H), 4.21 (d, *J* = 5.5 Hz, 1H), 4.35 (d, *J* = 12.5 Hz, 1H), 4.47 (d, *J* = 12.5 Hz, 1H), 4.53 (d, *J* = 12.0 Hz, 1H), 4.60 (dd, *J* = 4.0, 5.5 Hz, 1H), 4.74 (d, *J* = 12.0 Hz, 2H), 5.74 (d, *J* = 4.0 Hz, 1H), 7.19–7.67 (m, 20H). ^{13}C NMR (100 MHz, $CDCl_3$): δ 19.08, 26.15, 26.59, 26.80, 34.93, 59.78, 72.41, 73.37, 77.88, 79.26, 86.65, 104.16, 113.01, 127.50, 127.52, 127.57, 127.72, 127.80, 128.29, 128.32, 129.45, 133.87, 135.57, 138.08, 138.21. MS (FAB): *m/z* 675 (MNa^+). HRMS (FAB): calcd for $C_{40}H_{48}O_6SiNa$ (MNa^+) 675.3118, found 675.3115.

4.3. 1,2-Di-*O*-acetyl-3,5-di-*O*-benzyl-4-(2-*tert*-butyldiphenylsiloxyethyl)-D-ribofuranose (3)

Under nitrogen atmosphere, Ac_2O (10 mL, 110 mmol) and H_2SO_4 (0.1% in AcOH, 4.0 mL) were added to a solution of silyl ether **2** (5.86 g, 8.98 mmol) in AcOH (30 mL) at room temperature. The reaction mixture was stirred at room temperature for 2 h. The reaction was then quenched with satd $NaHCO_3$ aq and extracted with EtOAc. The combined organic layer was washed with satd $NaHCO_3$ aq, water and brine, dried over Na_2SO_4 and concentrated. The combined organic layer was washed with brine, dried over Na_2SO_4, and concentrated. The obtained crude residue (6.18 g) was purified by column chromatography (silica gel 200 g, *n*-hexane/EtOAc = 5:1) to give diacetate **3** as a colorless oil (5.67 g, 91%).

$[\alpha]_D^{24}$ −16.3 (*c* 1.00, $CHCl_3$). IR (KBr): 3069, 3031, 2931, 2857, 1748, 1496, 1472, 1455, 1428, 1369, 1309, 1219 cm^{-1}. ^{1}H NMR (400 MHz, $CDCl_3$): δ 1.02 (s, 9H), 1.83 (s, 3H), 1.93 (s, 3H), 1.96–2.13 (m, 2H), 3.39 (d, *J* = 10.0 Hz, 1H), 3.50 (d, *J* = 10.0 Hz, 1H), 3.81–3.93 (m, 2H), 4.36–4.44 (m, 3H), 4.46 (d, *J* = 12.0 Hz, 1H), 4.57 (d, *J* = 12.0 Hz, 1H), 5.28 (d, *J* = 5.5 Hz, 1H), 6.03 (s, 1H), 7.21–7.67 (m, 20H). ^{13}C NMR (100 MHz, $CDCl_3$): δ 19.09, 20.63, 20.93, 26.81, 35.75, 59.70, 73.16, 73.18, 73.44, 74.68, 78.07, 86.66, 97.61, 127.44, 127.49, 127.55, 127.57, 127.70, 127.75, 128.23, 128.32, 129.47, 133.87, 133.91, 135.53, 137.80, 138.15, 169.37, 169.70. MS (FAB): *m/z* 719 (MNa^+). HRMS (FAB): calcd for $C_{41}H_{48}O_8SiNa$ (MNa^+) 719.3016, found 719.2999.

4.4. 2′-*O*-Acetyl-3′,5′-di-*O*-benzyl-4′-(2-*tert*-butyldiphenylsiloxyethyl)-5-methyluridine (4)

Under nitrogen atmosphere, thymine (1.41 g, 11.2 mmol) and BSA (6.8 mL, 28 mmol) were added to a solution of diacetate **3** (4.36 g, 11.0 mmol) in MeCN (20 mL) at room temperature. The reaction mixture was refluxed for 1.5 h. TMSOTf (1.9 mL, 10 mmol) was added to the resulting mixture at 0 °C. The reaction mixture was refluxed for 3.5 h. The reaction was then quenched with satd $NaHCO_3$ aq and extracted with EtOAc. The combined organic layer was washed with water and brine, dried over Na_2SO_4, and concentrated. The obtained crude residue (5.71 g) was purified by column chromatography (silica gel 150 g, *n*-hexane/EtOAc = 3:2) to give acetate **4** as a white foam (5.14 g, 84%).

Mp: 45–48 °C. $[\alpha]_D^{25}$ +10.2 (*c* 1.00, $CHCl_3$). IR (KBr): 3172, 3068, 2930, 2857, 1747, 1693, 1470, 1428, 1372, 1234 cm^{-1}. ^{1}H NMR (400 MHz, $CDCl_3$): δ 1.01 (s, 9H), 1.48 (s, 3H), 1.76–1.83 (m, 1H), 2.04 (s, 3H), 2.03–2.11 (m, 1H), 3.41 (d, *J* = 10.5 Hz, 1H), 3.71–3.83 (m, 2H), 3.89 (d, *J* = 10.5 Hz, 1H), 4.35 (d, *J* = 6.5 Hz, 1H), 4.38 (d, *J* = 11.5 Hz, 1H), 4.39 (d, *J* = 9.5 Hz, 1H), 4.44 (d, *J* = 9.5 Hz, 1H), 4.57 (d, *J* = 11.5 Hz, 1H), 5.35 (dd, *J* = 5.0, 6.5 Hz, 1H), 6.08 (d, *J* = 5.0 Hz, 1H), 7.20–7.41 (m, 16H), 7.49 (s, 1H), 7.60–7.65 (m, 4H), 7.83 (br s, 1H). ^{13}C NMR (100 MHz, $CDCl_3$): δ 11.96, 19.06, 20.82, 26.82, 35.09, 59.27, 73.10, 73.38, 74.22, 75.24, 77.43, 86.03, 87.35, 111.21, 127.58, 127.66, 127.85, 128.01, 128.42, 128.59, 129.67, 133.47, 133.51, 135.51, 135.69, 137.32, 137.49, 150.28, 163.58, 170.05. MS (FAB): *m/z* 763 (MH^+). HRMS (FAB): calcd for $C_{44}H_{51}N_2O_8Si$ (MH^+) 763.3415, found 763.3402.

4.5. 3′,5′-Di-*O*-benzyl-4′-(2-*tert*-butyldiphenylsiloxyethyl)-5-methyluridine (5)

K_2CO_3 (450 mg, 330 mmol) was added to a solution of compound **4** (5.04 g, 6.61 mmol) in MeOH (10 mL) at room temperature. The reaction mixture was stirred at room temperature for 1 h. The reaction was then quenched with satd NH_4Cl aq and extracted with EtOAc. The combined organic layer was washed with water and brine, dried over Na_2SO_4, and concentrated. The obtained crude residue (4.76 g) was purified by column chromatography (silica gel 100 g, *n*-hexane/EtOAc = 4:3) to give alcohol **5** as a white foam 4.54 g, 95%).

Mp: 62–64 °C. $[\alpha]_D^{26}$ −10.3 (*c* 1.00, $CHCl_3$). IR (KBr): 3423, 3179, 3066, 2928, 2856, 1695, 1471, 1428, 1391, 1362, 1270 cm^{-1}. ^{1}H NMR (400 MHz, $CDCl_3$): δ 1.06 (s, 9H), 1.56 (s, 3H), 1.77 (ddd, *J* = 6.5, 8.0, 14.5 Hz, 1H), 2.14 (dt, *J* = 5.0, 14.5 Hz, 1H), 2.83 (d, *J* = 8.0 Hz, 1H), 3.45 (d, *J* = 10.5 Hz, 1H), 3.73–3.88 (m, 2H), 3.85 (d, *J* = 10.5 Hz, 1H), 4.14 (d, *J* = 6.0 Hz, 1H), 4.30 (m, 1H), 4.46 (d, *J* = 12.0 Hz, 1H), 4.49 (d, *J* = 12.0 Hz, 1H), 4.56 (d, *J* = 11.0 Hz, 1H), 4.63 (d, *J* = 11.0 Hz, 1H), 5.82 (d, *J* = 6.0 Hz, 1H), 7.22–7.65 (m,

21H), 8.12 (br s, 1H). ^{13}C NMR (100 MHz, $CDCl_3$): δ 12.04, 19.05, 26.83, 35.36, 59.36, 73.49, 74.05, 74.57, 75.02, 79.41, 87.03, 88.43, 111.93, 127.50, 127.64, 127.66, 128.01, 128.06, 128.25, 128.57, 128.60, 129.65, 129.68, 133.51, 135.52, 135.89, 137.02, 137.33, 150.80, 163.69. MS (FAB): *m/z* 721 (MH^+). HRMS (FAB): calcd for $C_{42}H_{49}N_2O_7Si$ (MH^+) 721.3309, found 721.3320.

4.6. 3′,5′-Di-*O*-benzyl-4′-(2-*tert*-butyldiphenylsiloxyethyl)-2′-*O*-methanesulfonyl-5-methyluridine (6)

Under nitrogen atmosphere, Et_3N (4.0 mL, 29 mmol) and MsCl (0.70 mL, 9.0 mmol) were added to a solution of alcohol **5** (3.26 g, 4.52 mmol) in CH_2Cl_2 (40 mL) at 0 °C. The reaction mixture was stirred at 0 °C for 1.5 h. The reaction was then quenched with satd $NaHCO_3$ aq at 0 °C and extracted with CH_2Cl_2. The combined organic layer was washed with water and brine, dried over Na_2SO_4, and concentrated. The obtained crude residue (3.80 g) was purified by column chromatography (silica gel 100 g, *n*-hexane/EtOAc = 4:3) to give mesylate **6** as a white foam (3.29 g, 91%).

Mp: 57–62 °C. $[\alpha]_D^{22}$ +214.8 (*c* 1.00, $CHCl_3$). IR (KBr): 3168, 3068, 3031, 2932, 2857, 1694, 1538, 1471, 1428, 1361, 1272 cm^{-1}. ^{1}H NMR (400 MHz, $CDCl_3$): δ 1.02 (s, 9H), 1.44 (s, 3H), 1.85 (ddd, *J* = 6.5, 8.0, 14.5 Hz, 1H), 2.10 (dt, *J* = 5.0, 14.5 Hz, 1H), 3.07 (s, 3H), 3.44 (d, *J* = 6.5 Hz, 1H), 3.70–3.86 (m, 2H), 3.95 (d, *J* = 6.5 Hz, 1H), 4.33 (d, *J* = 5.0 Hz, 1H), 4.37 (d, *J* = 12.0 Hz, 1H), 4.42 (d, *J* = 12.0 Hz, 1H), 4.45 (d, *J* = 12.0 Hz, 1H), 4.83 (d, *J* = 12.0 Hz, 1H), 5.26 (dd, *J* = 3.0, 5.0 Hz, 1H), 6.01 (d, *J* = 3.0 Hz, 1H), 7.18–7.63 (m, 21H), 8.29 (br s, 1H). ^{13}C NMR (75.5 MHz, $CDCl_3$): δ 11.90, 19.08, 26.85, 35.11, 38.83, 59.13, 72.65, 73.40, 73.78, 76.39, 80.30, 86.74, 87.83, 111.27, 127.60, 127.68, 127.70, 128.11, 128.12, 128.47, 128.64, 129.70, 129.73, 133.42, 133.46, 135.28, 135.53, 137.11, 137.22, 150.46, 163.44. MS (FAB): *m/z* 799 (MH^+). HRMS (FAB): calcd for $C_{43}H_{48}N_2O_9F_3SiS$ (MH^+) 799.3085, found 799.3085.

4.7. 3′,5′-Di-*O*-benzyl-4′-(2-*tert*-butyldiphenylsiloxyethyl)-5-methylarabinouridine (7)

1 M NaOH aq (12 mL, 12 mmol) was added to a solution of mesylate **6** (3.16 g, 3.95 mmol) in EtOH (40 mL) at room temperature. The reaction mixture was stirred at room temperature for 12 h. The reaction was then quenched with satd NH_4Cl aq at 0 °C and extracted with EtOAc. The combined organic layer was washed with water and brine, dried over Na_2SO_4, and concentrated. The obtained crude residue (2.72 g) was purified by column chromatography (silica gel 100 g, *n*-hexane/EtOAc = 1:1) to give alcohol **7** as a white foam (2.55 g, 89%).

Mp: 56–58 °C. $[\alpha]_D^{26}$ +43.5 (*c* 1.00, $CHCl_3$). IR (KBr): 3357, 3181, 3068, 3031, 2929, 2856, 1695, 1472, 1455, 1428, 1390, 1362, 1281 1206 cm^{-1}. ^{1}H NMR (300 MHz, $CDCl_3$): δ 1.02 (s, 9H), 1.71 (d, *J* = 1.0 Hz, 3H), 1.88–1.93 (m, 2H), 3.52 (d, *J* = 10.5 Hz, 1H), 3.72–3.86 (m, 2H), 3.91 (d, *J* = 10.5 Hz, 1H), 4.14 (d, *J* = 4.0 Hz, 1H), 4.26 (d, *J* = 8.0 Hz, 1H), 4.39 (ddd, *J* = 4.0, 5.0, 8.0 Hz, 1H), 4.45 (d, *J* = 12.0 Hz, 1H), 4.49 (d, *J* = 11.5 Hz, 1H), 4.51 (d, *J* = 11.5 Hz, 1H), 4.74 (d, *J* = 12.0 Hz, 1H), 5.96 (d, *J* = 5.0 Hz, 1H), 7.21–7.65 (m, 20H), 7.48 (d, *J* = 1.0 Hz, 1H), 9.01 (br s, 1H). ^{13}C NMR (100 MHz, $CDCl_3$): δ 12.27, 19.09, 26.86, 35.16, 59.59, 72.65, 73.18, 73.70, 74.66, 83.80, 84.65, 85.07, 109.27, 127.66, 127.83, 127.93, 128.33, 128.39, 128.70, 129.69, 129.72, 133.44, 135.50, 136.62, 137.40, 137.55, 150.67, 163.99. MS (FAB): *m/z* 721 (MH^+). HRMS (FAB): calcd for $C_{42}H_{49}N_2O_7Si$ (MH^+) 721.3309, found 721.3300.

4.8. 3′,5′-Di-*O*-benzyl-4′-(2-*tert*-butyldiphenylsiloxyethyl)-5-methyl-2′-*O*-(trifluoromethanesulfonyl)arabinouridine (8)

Under nitrogen atmosphere, pyridine (1.9 mL, 17 mmol) and Tf_2O (1.4 mL, 8.6 mmol) were added to a solution of alcohol **7** (2.07 g, 2.87 mmol) in CH_2Cl_2 (30 mL) at 0 °C. The reaction mixture was stirred at 0 °C for 0.5 h. The reaction was then quenched with satd $NaHCO_3$ aq at 0 °C and extracted with CH_2Cl_2. The combined organic layer was washed with water and brine, dried over Na_2SO_4, and concentrated. The obtained crude residue (2.56 g) was purified by column chromatography (silica gel 100 g, *n*-hexane/EtOAc = 2:1) to give triflate **8** as a white foam (2.03 g, 83%).

Mp: 37–40 °C. $[\alpha]_D^{25}$ +37.1 (*c* 1.00, $CHCl_3$). IR (KBr): 3190, 3069, 2930, 2858, 1695, 1455, 1426, 1245, 1215, 1143 cm^{-1}. ^{1}H NMR (400 MHz, $CDCl_3$): δ 1.03 (s, 9H), 1.67 (s, 3H), 1.81–1.95 (m, 2H), 3.36 (d, *J* = 10.5 Hz, 1H), 3.69 (d, *J* = 10.5 Hz, 1H), 3.72–3.86 (m, 2H), 4.38 (d, *J* = 12.0 Hz, 1H), 4.43 (d, *J* = 12.0 Hz, 1H), 4.48 (d, *J* = 11.5 Hz, 1H), 4.57 (d, *J* = 4.5 Hz, 1H), 4.72 (d, *J* = 11.5 Hz, 1H), 5.35 (dd, *J* = 4.5, 5.5 Hz, 1H), 6.19 (d, *J* = 5.5 Hz, 1H), 7.19–7.63 (m, 21H), 8.10 (br s, 1H). ^{13}C NMR (100 MHz, $CDCl_3$): δ 12.21, 19.00, 26.77, 34.04, 59.04, 71.23, 73.32, 73.47, 80.48, 81.51, 84.37, 87.53, 110.98, 118.24 (q, *J* = 318 Hz), 127.64, 127.67, 127.69, 127.98, 128.01, 128.33, 128.45, 128.53, 129.72, 129.79, 133.26, 133.28, 135.47, 135.49, 136.41, 137.12, 150.13, 163.48. MS (FAB): *m/z* 853 (MH^+). HRMS (FAB): calcd for $C_{43}H_{48}N_2O_9F_3SiS$ (MH^+) 853.2802, found 853.2813.

4.9. (2′*R*)-2′-Azido-3′,5′-di-*O*-benzyl-4′-(2-*tert*-butyldiphenylsiloxyethyl)thymidine (9)

Under nitrogen atmosphere, NaN_3 (464 mg, 7.14 mmol) was added to a solution of triflate **8** (2.03 g, 2.38 mmol) in DMF (20 mL) at room temperature. The reaction mixture was stirred at room temperature for 13 h. The resulting mixture was added to water and extracted with Et_2O. The combined organic layer was washed with brine, dried over Na_2SO_4, and concentrated. The obtained crude residue (2.20 g) was purified by column chromatography (silica gel 150 g, *n*-hexane/EtOAc = 2:1) to give azide **9** as a white foam (1.80 g, quant.).

Mp: 46–49 °C. $[\alpha]_D^{25}$ −5.1 (*c* 1.00, $CHCl_3$). IR (KBr): 3179, 3068, 2929, 2857, 2109, 1694, 1470, 1428, 1362, 1268 cm^{-1}. ^{1}H NMR (400 MHz, $CDCl_3$): δ 1.03 (s, 9H), 1.58 (d, *J* = 1.0 Hz, 3H), 1.78 (ddd, *J* = 6.0, 8.0, 14.5 Hz, 1H), 2.15 (ddd, *J* = 5.0, 5.5, 14.5 Hz, 1H), 3.44 (d, *J* = 11.0 Hz, 1H), 3.70–3.85 (m, 2H), 3.91 (d, *J* = 11.0 Hz, 1H), 3.97 (t, *J* = 6.0 Hz, 1H), 4.28 (d, *J* = 6.0 Hz, 1H), 4.43 (d, *J* = 11.5 Hz, 1H), 4.49 (d, *J* = 11.5 Hz, 1H), 4.49 (d, *J* = 11.5 Hz, 1H), 4.79 (d, *J* = 11.5 Hz, 1H), 5.99 (d, *J* = 6.0 Hz, 1H), 7.20–7.64 (m, 20H), 7.49 (d, *J* = 1.0 Hz, 1H), 7.93 (br s, 1H). ^{13}C NMR (100 MHz, $CDCl_3$): δ 12.10, 19.04, 26.82, 35.22, 59.26, 65.17, 73.41, 73.47, 74.28, 79.06, 86.00, 87.57, 111.09, 127.55, 127.64, 127.66, 128.05, 128.12, 128.21, 128.51, 128.64, 129.66, 129.71, 133.43, 133.44, 135.24, 135.50, 136.90, 137.13, 150.25, 163.66. MS (FAB): *m/z* 746 (MH^+). HRMS (FAB): calcd for $C_{42}H_{48}N_5O_6Si$ (MH^+) 746.3374, found 746.3404.

4.10. (2′*R*)-2′-Azido-3′,5′-di-*O*-benzyl-4′-(2-hydroxyethyl) thymidine (10)

Under nitrogen atmosphere, TBAF (1.0 M in THF, 2.6 mL, 2.6 mmol) was added to a solution of azide **9** (1.78 g, 2.38 mmol) in THF (20 mL) at room temperature. The reaction mixture was stirred at room temperature for 17 h. The resulting mixture was added to water and extracted with EtOAc. The combined organic layer was washed with brine, dried over Na_2SO_4, and concentrated. The obtained crude residue (2.20 g) was purified by column chromatography (silica gel 75 g, *n*-hexane/EtOAc = 1:1) to give compound **10** as a white foam (1.22 g, quant.).

Mp: 45–50 °C. $[\alpha]_D^{25}$ +10.2 (*c* 1.00, $CHCl_3$). IR (KBr): 3441, 3182, 3063, 2927, 2109, 1693, 1496, 1469, 1455, 1364, 1267 cm^{-1}. ^{1}H NMR (400 MHz, $CDCl_3$): δ 1.56 (s, 3H), 1.66 (br s, 1H), 1.76 (dt, *J* = 6.0, 15.0 Hz, 1H), 2.21 (dt, *J* = 6.0, 15.0 Hz, 1H), 3.44 (d,

J = 10.5 Hz, 1H), 3.75 (t, J = 6.0 Hz, 2H), 3.82 (d, J = 10.5 Hz, 1H), 4.04 (t, J = 6.0 Hz, 1H), 4.30 (d, J = 6.0 Hz, 1H), 4.47 (d, J = 11.5 Hz, 1H), 4.53 (d, J = 11.5 Hz, 1H), 4.55 (d, J = 12.0 Hz, 1H), 4.83 (d, J = 12.0 Hz, 1H), 6.10 (d, J = 6.0 Hz, 1H), 7.22–7.38 (m, 10H), 7.44 (s, 1H), 8.34 (br s, 1H). ^{13}C NMR (100 MHz, $CDCl_3$): δ 12.12, 34.83, 58.28, 64.83, 73.32, 73.66, 74.50, 79.56, 86.30, 87.81, 111.36, 127.67, 128.11, 128.27, 128.37, 128.61, 128.72, 135.19, 136.72, 136.96, 150.22, 163.39. MS (FAB): m/z 508 (MH^+). HRMS (FAB): calcd for $C_{26}H_{30}N_5O_6$ (MH^+) 508.2196, found 508.2204.

4.11. (2′*R*)-2′-Azido-3′,5′-di-*O*-benzyl-4′-(2-carboxymethyl) thymidine (11)

MS4Å (3.0 g) and PDC (10.9 g, 28.8 mmol) were added to a solution of compound **10** (1.22 g, 2.38 mmol) in DMF (20 mL) at room temperature. The reaction mixture was stirred at room temperature for 12 h. The resulting mixture was added to water and AcOH and extracted with EtOAc. The combined organic layer was washed with 0.4 M $(COOH)_2$ aq, 0.2 M $(COONH_4)_2$ aq, and brine, dried over Na_2SO_4, and concentrated. The obtained crude residue (3.20 g) was purified by column chromatography (silica gel 75 g, *n*-hexane/EtOAc/AcOH = 50:50:1) to give carboxylic acid **11** as a white foam (1.18 g, 94%).

Mp: 78–81 °C. $[\alpha]_D^{25}$ −29.4 (*c* 1.00, $CHCl_3$). IR (KBr): 3510, 3179, 3033, 2929, 2108, 1705, 1470, 1455, 1269, 1213 cm^{-1}. ^{1}H NMR (400 MHz, $CDCl_3$): δ 1.56 (s, 3H), 2.71 (d, J = 16.5 Hz, 1H), 2.88 (d, J = 16.5 Hz, 1H), 3.77 (d, J = 10.0 Hz, 1H), 3.94 (d, J = 10.0 Hz, 1H), 3.99 (dd, J = 5.5, 7.0 Hz, 2H), 4.37 (d, J = 5.5 Hz, 1H), 4.49 (d, J = 11.0 Hz, 1H), 4.53 (d, J = 10.5 Hz, 1H), 4.61 (d, J = 10.5 Hz, 1H), 4.88 (d, J = 11.0 Hz, 1H), 6.22 (d, J = 7.0 Hz, 1H), 7.20–7.48 (m, 11H), 9.65 (br s, 1H). ^{13}C NMR (100 MHz, $CDCl_3$): δ 12.14, 38.05, 64.99, 73.80, 73.99, 75.30, 80.26, 85.30, 86.36, 111.74, 127.81, 128.06, 128.19, 128.46, 128.52, 128.89, 135.59, 136.81, 137.02, 150.67, 164.38, 175.09. MS (FAB): m/z 522 (MH^+). HRMS (FAB): calcd for $C_{26}H_{28}N_5O_7$ (MH^+) 522.1989, found 522.1979.

4.12. (2′*R*)-2′-Amino-3′,5′-di-*O*-benzyl-4′-(2-carboxymethyl) thymidine (12) and (2′*R*)-3′,5′-Di-*O*-benzyl-2′,4′-(2-oxo-iminoethano)thymidine (13)

Reduction by $NaBH_4$: Under nitrogen atmosphere, $NaBH_4$ (56.2 mg, 1.49 mmol) was added to a solution of carboxylic acid **11** (155 mg, 0.297 mmol) in *i*-PrOH (3.0 mL) at 0 °C. The reaction mixture was refluxed for 1 h. The reaction was then quenched with acetone and the resulting mixture was concentrated. The obtained crude residue (220 mg) was purified by column chromatography (silica gel 5.0 g, $CHCl_3$/MeOH = 20:1) to give compound **12** as a white foam (81.3 mg, 55%).

Staudinger reaction: Under nitrogen atmosphere, Me_3P (1.0 M in toluene, 0.55 mL, 0.55 mmol) was added to a solution of carboxylic acid **11** (241 mg, 0.462 mmol) in THF/H_2O (5:1, 6.0 mL) at room temperature. The reaction mixture was stirred at room temperature for 24 h. The resulting mixture was concentrated. The obtained crude residue (293 mg) was purified by column chromatography (silica gel 10 g, $CHCl_3$/MeOH = 30:1) to give lactam **13** as a white foam (106 mg, 43%) together with compound **12** (81 mg, ca. 35%) including a small amount of impurity.

Condensation using EDC: Under nitrogen atmosphere, EDC (157 mg, 0.820 mmol) and DMAP (10.0 mg, 0.0820 mmol) were added to a solution of amino acid **12** (81.3 mg, 0.164 mmol) in CH_2Cl_2 (3.0 mL) at 0 °C. The reaction mixture was stirred at room temperature for 24 h. The reaction was then quenched with satd $NaHCO_3$ aq at 0 °C and extracted with CH_2Cl_2. The combined organic layer was washed with water and brine, dried over Na_2SO_4, and concentrated. The obtained crude residue (65.4 mg) was purified by column chromatography (silica gel 3.0 g, $CHCl_3$/MeOH = 20:1) to give lactam **13** as a white foam (56.6 mg, 72%).

Condensation using MsCl: Under nitrogen atmosphere, Et_3N (0.32 mL, 2.25 mmol) and MsCl (70 μL, 0.0820 mmol) were added to a solution of amino acid **12** (223 mg, 0.450 mmol) in CH_2Cl_2 (5.0 mL) at 0 °C. The reaction mixture was stirred at room temperature for 17 h. The reaction was then quenched with satd $NaHCO_3$ aq at 0 °C and extracted with CH_2Cl_2. The combined organic layer was washed with water and brine, dried over Na_2SO_4, and concentrated. The obtained crude residue (300 mg) was purified by column chromatography (silica gel 10 g, $CHCl_3$/MeOH = 20:1) to give lactam **13** as a white foam (185 mg, 86%).

Compound **12**: Mp: 45–48 °C. $[\alpha]_D^{26}$ −12.2 (*c* 1.00, $CHCl_3$). IR (KBr): 3426, 3197, 3033, 2925, 2878, 1697, 1497, 1473, 1455, 1390, 1274, 1213 cm^{-1}. ^{1}H NMR (400 MHz, CD_3OD): δ 1.65 (s, 3H), 2.84 (s, 2H), 3.84 (d, J = 9.5 Hz, 1H), 3.92 (d, J = 9.5 Hz, 1H), 4.19–4.20 (m, 1H), 4.61–4.85 (m, 5H), 6.22 (d, J = 8.0 Hz, 1H), 7.25–7.42 (m, 10H), 7.55 (s, 1H), 7.90 (br s, 1H). ^{13}C NMR (100 MHz, CD_3OD): δ 12.48, 38.19, 57.92, 74.79, 75.07, 76.89, 81.36, 86.89, 89.23, 112.37, 128.66, 128.79, 128.97, 129.10, 129.19, 129.72, 136.82, 138.01, 138.86, 152.64, 165.92, 173.68. MS (FAB): m/z 496 (MH^+). HRMS (FAB): calcd for $C_{26}H_{30}N_3O_7$ (MH^+) 496.2084, found 496.2081.

Compound **13**: Mp: 112–114 °C. $[\alpha]_D^{21}$ +78.9 (*c* 1.00, $CHCl_3$). IR (KBr): 3500, 3169, 3063, 2926, 1685, 1454, 1367, 1273, 1211 cm^{-1}. ^{1}H NMR (300 MHz, $CDCl_3$): δ 1.37 (d, J = 1.0 Hz, 3H), 2.40 (d, J = 18.0 Hz, 1H), 2.58 (d, J = 18.0 Hz, 1H), 3.60 (d, J = 11.0 Hz, 1H), 3.72 (d, J = 11.0 Hz, 1H), 4.23 (dd, J = 4.0, 6.0 Hz, 2H), 4.32 (d, J = 4.0 Hz, 1H), 4.54 (d, J = 11.5 Hz, 1H), 4.56 (d, J = 11.5 Hz, 1H), 4.60 (d, J = 11.5 Hz, 1H), 4.71 (d, J = 11.5 Hz, 1H), 5.83 (s, 1H), 7.25–7.35 (m, 11H), 7.94 (d, J = 1.0 Hz, 1H), 9.40 (br s, 1H). ^{13}C NMR (100 MHz, $CDCl_3$): δ 11.96, 38.60, 55.75, 68.71, 70.57, 71.96, 73.57, 83.78, 90.10, 109.61, 127.56, 127.89, 127.97, 128.23, 128.43, 128.66, 135.54, 136.96, 137.07, 150.72, 164.25, 169.56. MS (FAB): m/z 478 (MH^+). HRMS (FAB): calcd for $C_{26}H_{28}N_3O_6$ (MH^+) 478.1978, found 478.1983.

4.13. (2′*R*)-2′,4′-(2-Oxo-iminoethano)thymidine (15)

Lactam **13** (50.0 mg, 0.105 mmol) in MeOH (2.0 mL) was added to a suspension of 20% $Pd(OH)_2$ on carbon (50.0 mg, 0.462 mmol) in MeOH (1.0 mL) at room temperature under nitrogen atmosphere. The reaction mixture was stirred at room temperature for 24 h under hydrogen atmosphere. The resulting mixture was filtered and concentrated. The obtained crude residue (25.4 mg) was purified by recrystallization from MeOH to give nucleoside **15** as a white solid (19.1 mg, 61%).

Mp: 187–188 °C. $[\alpha]_D^{23}$ +36.5 (*c* 0.200, CH_3OH); IR (KBr): 3449, 3318, 3175, 3060, 2926, 2819, 1707, 1651, 1469, 1386, 1272, 1215 cm^{-1}. ^{1}H NMR (300 MHz, CD_3OD): δ 1.85 (s, 3H), 2.29 (d, J = 18.0 Hz, 1H), 2.46 (d, J = 18.0 Hz, 1H), 3.68 (d, J = 12.5 Hz, 1H), 3.75 (d, J = 12.5 Hz, 1H), 3.82 (d, J = 4.0 Hz, 1H), 4.33 (d, J = 4.0 Hz, 1H), 5.68 (s, 1H), 8.35 (s, 1H). ^{13}C NMR (100 MHz, CD_3OD): δ 12.55, 38.80, 60.02, 61.82, 64.42, 85.99, 91.01, 110.08, 137.78, 152.07, 166.63, 173.32. MS (FAB): m/z 298 (MH^+). HRMS (FAB): calcd for $C_{26}H_{28}N_3O_6$ (MH^+) 298.1039, found 298.1044.

4.14. (2′*R*)-5′-*O*-(4,4′-Dimethoxytrityl)-2′,4′-(2-oxo-iminoethano)thymidine (16)

Under nitrogen atmosphere, DMTrCl (95.7 mg, 0.283 mmol) was added to a solution of nucleoside **15** (28.0 mg, 0.0941 mmol) in pyridine (2.0 mL) at 0 °C. The reaction mixture was stirred at room temperature for 3 h. The reaction was then quenched with satd $NaHCO_3$ aq at 0 °C and extracted with EtOAc. The combined organic layer was washed with water and brine, dried over Na_2SO_4, and concentrated. The obtained crude residue (159 mg) was purified by column chromatography (silica gel 5.0 g, $CHCl_3$/MeOH = 20:1) to give compound **16** as a white foam (45.9 mg, 81%).

Mp: 204–206 °C. $[\alpha]_D^{23}$ +80.7 (*c* 1.00, $CHCl_3$). IR (KBr): 3563, 3341, 3062, 2933, 2838, 1705, 1657, 1608, 1509, 1466, 1384, 1254 cm^{-1}. ^1H NMR (300 MHz, CD_3OD): δ 1.20 (d, J = 1.0 Hz, 3H), 2.37 (d, J = 18.0 Hz, 1H), 2.44 (d, J = 18.0 Hz, 1H), 3.33 (d, J = 11.0 Hz, 1H), 3.37 (d, J = 11.0 Hz, 1H), 3.74 (s, 6H), 3.94 (d, J = 4.0 Hz, 1H), 4.56 (d, J = 4.0 Hz, 1H), 5.66 (s, 1H), 6.83–7.47 (m, 13H), 7.86 (d, J = 1.0 Hz, 1H). ^{13}C NMR (75 MHz, CD_3OD): δ 12.28, 39.32, 55.72, 59.82, 64.37, 65.71, 85.55, 88.06, 91.70, 110.67, 114.28, 128.19, 129.03, 129.44, 131.45, 136.38, 136.59, 136.87, 145.75, 152.01, 160.32, 160.35, 166.52, 173.00. MS (FAB): *m/z* 600 (MH^+). HRMS (FAB): calcd for $C_{26}H_{28}N_3O_6$ (MH^+) 600.2346, found 600.2347.

4.15. (2′*R*)-3′-*O*-[2-Cyanoethoxy(diisopropylamino)phosphino]-5′-*O*-(4,4′-dimethoxytrityl)-2′,4′-(2-oxo-iminoethano)thymidine (14)

Under nitrogen atmosphere, 1*H*-tetrazole (10.1 mg, 0.144 mmol) and $(i\text{-}Pr_2N)_2POCH_2CH_2CN$ (46 μL, 0.14 mmol) were added to a solution of compound **16** (72.0 mg, 0.120 mmol) in THF/MeCN (3:1, 2.0 mL) at 0 °C. The reaction mixture was stirred at room temperature for 12 h. The reaction was then quenched with satd $NaHCO_3$ aq at 0 °C and extracted with CH_2Cl_2. The combined organic layer was washed with satd $NaHCO_3$ aq, water and brine, dried over Na_2SO_4, and concentrated. The obtained crude residue (99.0 mg) was purified by column chromatography (silica gel 3.0 g, $CHCl_3$/MeOH = 20:1) to give **14** as a white foam (70.2 mg, 73%).

Mp: 127–129 °C. ^1H NMR (400 MHz, $CDCl_3$): δ 0.99 (d, J = 7.0 Hz, 1.8H), 1.09 (d, J = 7.0 Hz, 4.2 H), 1.10 (d, J = 7.0 Hz, 4.2H), 1.16 (d, J = 7.0 Hz, 1.8H), 1.23 (s, 0.9H), 1.26 (s, 2.1H), 2.36–2.64 (m, 4H), 3.24–3.81 (m, 12H), 4.18 (dd, J = 4.0, 6.0 Hz, 0.3H), 4.32 (dd, J = 4.0, 5.5 Hz, 0.7H), 4.62 (dd, J = 4.0, 7.0 Hz, 0.3H), 4.76 (dd, J = 4.0, 7.0 Hz, 0.7H), 5.74 (s, 0.7H), 5.76 (s, 0.3H), 6.28 (d, J = 5.5 Hz, 0.7H), 6.33 (d, J = 6.0 Hz, 0.3H), 6.82–7.47 (m, 13H), 7.83 (s, 1H), 8.27 (br s, 1H). ^{31}P NMR (160 MHz, $CDCl_3$): δ 148.70, 150.53. MS (FAB): *m/z* 800 (MH^+), HRMS (FAB): calcd for $C_{42}H_{51}N_5O_9P$ (MH^+) 800.3424, found 800.3406.

4.16. (2′*R*)-3-Benzyloxymethyl-3′,5′-di-*O*-benzyl-2′,4′-(2-oxo-iminoethano)thymidine (18)

Under nitrogen atmosphere, DBU (0.12 mL, 0.79 mmol) and BOMCl (55 μL, 0.39 mmol) were added to a solution of lactam **13** (94.0 mg, 0.197 mmol) in DMF (2.0 mL) at 0 °C. The reaction mixture was stirred at 0 °C for 0.5 h. The reaction was then quenched with satd $NaHCO_3$ aq at 0 °C and extracted with EtOAc. The combined organic layer was washed with water and brine, dried over Na_2SO_4, and concentrated. The obtained crude residue (112 mg) was purified by column chromatography (silica gel 5.0 g, *n*-hexane/EtOAc = 1:1) to give compound **18** as a white foam (101 mg, 86%).

Mp: 66–68 °C. $[\alpha]_D^{28}$ +79.7 (*c* 1.00, $CHCl_3$). IR (KBr): 3070, 3032, 2924, 2819, 1703, 1661, 1496, 1454, 1364, 1274, 1212 cm^{-1}. ^1H NMR (400 MHz, $CDCl_3$): δ 1.43 (d, J = 1.0 Hz, 3H), 2.45 (d, J = 17.5 Hz, 1H), 2.60 (d, J = 17.5 Hz, 1H), 3.59 (d, J = 10.5 Hz, 1H), 3.76 (d, J = 10.5 Hz, 1H), 3.96 (dd, J = 4.0, 5.5 Hz, 1H), 4.19 (d, J = 4.0 Hz, 1H), 4.51 (d, J = 11.0 Hz, 1H), 4.55 (d, J = 11.0 Hz, 1H), 4.60 (d, J = 11.0 Hz, 1H), 4.63 (d, J = 11.0 Hz, 1H), 4.69 (s, 2H), 5.43 (d, J = 9.5 Hz, 1H), 5.46 (d, J = 9.5 Hz, 1H), 5.74 (s, 1H), 6.15 (d, J = 5.5 Hz, 1H), 7.25–7.38 (m, 15H), 7.92 (d, J = 1.0 Hz, 1H). ^{13}C NMR (100 MHz, $CDCl_3$): δ 12.53, 38.68, 56.09, 68.73, 70.27, 70.57, 72.27, 72.37, 73.69, 83.76, 90.53, 109.48, 127.55, 127.64, 127.71, 127.91, 128.30, 128.34, 128.58, 128.73, 133.97, 136.59, 136.88, 137.82, 150.79, 163.29, 169.26. MS (FAB): *m/z* 598 (MH^+). HRMS (FAB): calcd for $C_{34}H_{36}N_3O_7$ (MH^+) 598.2553, found 598.2529.

4.17. (2′*R*)-3-Benzyloxymethyl-3′,5′-di-*O*-benzyl-2′,4′-(*N*-methyl-2-oxo-iminoethano)thymidine (19)

Under nitrogen atmosphere, 60% NaH (in mineral oil, 10.4 mg, 0.260 mmol) was added to a solution of compound **18** (130 mg, 0.218 mmol) in DMF (2.0 mL) at 0 °C. The reaction mixture was stirred at 0 °C for 0.5 h. MeI (68 μL, 1.1 mmol) was added to the resulting mixture at 0 °C. The reaction mixture was stirred at 0 °C for 2 h. The reaction was then quenched with satd $NaHCO_3$ aq at 0 °C and extracted with Et_2O. The combined organic layer was washed with brine, dried over Na_2SO_4, and concentrated. The obtained crude residue (139 mg) was purified by column chromatography (silica gel 5.0 g, *n*-hexane/EtOAc = 3:2) to give *N*-Me lactam **19** as a white foam (79.6 mg, 60%).

Mp: 48–50 °C. $[\alpha]_D^{28}$ +67.8 (*c* 0.760, $CHCl_3$). IR (KBr): 3065, 3031, 2925, 2819, 1707, 1651, 1496, 1453, 1365, 1279, 1212 cm^{-1}. ^1H NMR (400 MHz, $CDCl_3$): δ 1.45 (d, J = 1.0 Hz, 3H), 2.42 (d, J = 17.0 Hz, 1H), 2.60 (d, J = 17.0 Hz, 1H), 3.07 (s, 3H), 3.68 (d, J = 12.0 Hz, 1H), 3.74 (d, J = 12.0 Hz, 1H), 3.82 (d, J = 4.0 Hz, 1H), 4.16 (d, J = 4.0 Hz, 1H), 4.54–4.61 (m, 4H), 4.70 (s, 2H), 5.43 (d, J = 9.5 Hz, 1H), 5.47 (d, J = 9.5 Hz, 1H), 5.66 (s, 1H), 7.23–7.39 (m, 15H), 7.91 (d, J = 1.0 Hz, 1H). ^{13}C NMR (100 MHz, $CDCl_3$): δ 12.55, 34.17, 38.77, 63.11, 68.51, 70.20, 71.19, 72.27, 72.72, 73.64, 84.24, 88.87, 109.38, 127.52, 127.66, 127.70, 127.89, 128.27, 128.30, 128.32, 128.62, 128.69, 133.93, 136.69, 136.92, 137.81,150.68, 163.35, 167.29. MS (FAB): *m/z* 612 (MH^+). HRMS (FAB): calcd for $C_{35}H_{38}N_3O_7$ (MH^+) 612.2710, found 612.2712.

4.18. (2′*R*)-2′,4′-(*N*-Methyl-2-oxo-iminoethano)thymidine (20)

Under nitrogen atmosphere, *N*-Me lactam **19** (79.6 mg, 0.130 mmol) in EtOH (8.0 mL) and cyclohexene (1.3 mL, 13 mmol) were added to a suspension of 20% $Pd(OH)_2$ on carbon (91.0 mg) in EtOH (2.0 mL) at room temperature. The reaction mixture was refluxed for 2 h. The resulting mixture was filtered and concentrated. The obtained crude residue was purified by column chromatography (silica gel 2.0 g, $CHCl_3$/MeOH = 10:1) to give nucleoside **20** as a white powder (40.8 mg, quant.).

Mp: >300 °C. $[\alpha]_D^{28}$ +85.0 (*c* 1.40, CH_3OH). IR (KBr): 3430, 3301, 3175, 2925, 1705, 1473, 1386, 1273, 1215 cm^{-1}. ^1H NMR (400 MHz, CD_3OD): δ 1.77 (d, J = 1.0 Hz, 3H), 2.21 (d, J = 18.0 Hz, 1H), 2.39 (d, J = 18.0 Hz, 1H), 3.02 (s, 3H), 3.57 (d, J = 12.5 Hz, 1H), 3.64 (d, J = 12.5 Hz, 1H), 3.80 (d, J = 4.0 Hz, 1H), 4.23 (d, J = 4.0 Hz, 1H), 5.60 (s, 1H), 8.18 (d, J = 1.0 Hz, 1H). ^{13}C NMR (100 MHz, CD_3OD): δ 12.55, 34.92, 39.01, 61.60, 64.86, 67.68, 86.54, 89.33, 110.19, 137.47, 152.07, 166.65, 170.81. MS (FAB): *m/z* 312 (MH^+). HRMS (FAB): calcd for $C_{13}H_{18}N_3O_6$ (MH^+) 312.1196, found 312.1207.

4.19. (2′*R*)-5′-*O*-(4,4′-Dimethoxytrityl)-2′,4′-(*N*-methyl-2-oxo-iminoethano)thymidine (21)

Under nitrogen atmosphere, DMTrCl (175 mg, 0.567 mmol) was added to a solution of nucleoside **20** (26.8 mg, 0.0861 mmol) in pyridine (2.0 mL) at 0 °C. The reaction mixture was stirred at room temperature for 17 h. The reaction was then quenched with satd $NaHCO_3$ aq at 0 °C and extracted with CH_2Cl_2. The combined organic layer was washed with water and brine, dried over Na_2SO_4, and concentrated. The obtained crude residue (320 mg) was purified by column chromatography (silica gel 5.0 g, $CHCl_3$/MeOH = 25:1) to give compound **21** as a white foam (36.6 mg, 69%).

Mp: 155–157 °C. $[\alpha]_D^{26}$ +6.1 (*c* 2.10, $CHCl_3$). IR (KBr): 3350, 3198, 3087, 3006, 2933, 2836, 1694, 1651, 1508, 1464, 1392, 1350, 1254 cm^{-1}. ^1H NMR (300 MHz, $CDCl_3$): δ 1.30 (s, 3H), 2.44 (d, J = 17.5 Hz, 1H), 2.54 (d, J = 17.5 Hz, 1H), 3.09 (s, 3H), 3.33 (d, J = 11.0 Hz, 1H), 3.38 (d, J = 11.0 Hz, 1H), 3.75 (s, 3H), 3.76 (s, 3H),

3.94 (d, J = 4.0 Hz, 1H), 4.28 (br s, 1H), 4.49 (br s, 1H), 5.61 (s, 1H), 6.80–7.42 (m, 13H), 7.75 (s, 1H), 7.90 (br s, 1H). ^{13}C NMR (75 MHz, $CDCl_3$): δ 11.91, 34.51, 38.54, 55.20, 62.87, 65.43, 65.98, 84.96, 86.88, 88.60, 110.39, 111.34, 127.20, 128.07, 130.10, 134.92, 135.08, 144.05, 152.35, 158.69, 164.37, 168.32. MS (FAB): m/z 614 (MH^+). HRMS (FAB): calcd for $C_{34}H_{36}N_3O_8$ (MH^+) 614.2502, found 614.2496.

4.20. (2′*R*)-3′-*O*-[2-Cyanoethoxy(diisopropylamino)phosphino]-5′-*O*-(4,4′-dimethoxytrityl)-2′,4′-(*N*-methyl-2-oxo-iminoethano)thymidine (17)

Under nitrogen atmosphere, DIPEA (10.1 mg, 0.144 mmol) and *i*-$Pr_2NP(Cl)OCH_2CH_2CN$ (46 μL, 0.14 mmol) were added to a solution of compound **21** (72.0 mg, 0.120 mmol) in CH_2Cl_2 (2.0 mL) at 0 °C. The reaction mixture was stirred at room temperature for 2 h. The reaction was then quenched with satd $NaHCO_3$ aq at 0 °C and extracted with CH_2Cl_2. The combined organic layer was washed with satd $NaHCO_3$ aq, water, and brine, dried over Na_2SO_4, and concentrated. The obtained crude residue (99.0 mg) was purified by column chromatography (silica gel 3.0 g, $CHCl_3$/MeOH = 20:1) to give **17** as a white foam (70.2 mg, 73%).

Mp: 109–111 °C. ^{1}H NMR (400 MHz, $CDCl_3$): δ 0.99 (d, J = 7.0 Hz, 3.0H), 1.07 (d, J = 7.0 Hz, 3.0H), 1.11 (d, J = 7.0 Hz, 3.0H), 1.16 (d, J = 7.0 Hz, 3.0H), 1.26 (s, 1.5H), 1.29 (s, 1.5H), 2.36–2.64 (m, 4H), 3.17 (s, 3H), 3.22–3.88 (m, 12H), 4.10 (d, J = 4.5 Hz, 0.5H), 4.27 (d, J = 4.5 Hz, 0.5H), 4.60 (dd, J = 4.5, 7.0 Hz, 0.5H), 4.75 (dd, J = 4.0, 6.5 Hz, 0.5H), 5.67 (s, 0.5H), 5.69 (s, 0.5H), 6.82–7.47 (m, 13H), 7.83 (s, 1H), 8.27 (br s, 1H). ^{31}P NMR (400 MHz, $CDCl_3$): δ 148.86, 149.97. MS (FAB): m/z 814 (MH^+). HRMS (FAB): calcd for $C_{43}H_{53}N_5O_9P$ (MH^+) 814.3581, found 814.3599.

4.21. Oligonucleotide synthesis

Phosphoramidites **14** and **17** were used and the 0.2 μmol scale synthesis of oligonucleotides was performed on an automated DNA synthesizer (Gene Design nS-8) using a standard phosphoramidite protocol (DMTr-ON mode). Oligonucleotides **22–29** were prepared by cleavage from the CPG supports and deprotection of the phosphate moieties (28% NH_4 aq, rt, 1.5 h or 50 mM K_2CO_3 in MeOH, rt, 2 h). Removal of ammonia was carried out in vacuo. In the case of K_2CO_3 treatment, after neutralization with 1% HCl aq, the solvent was concentrated in vacuo. The crude **22–29** were purified with Sep-Pak® Plus C18 cartridges (Waters), followed by reversed-phase HPLC (Waters XBridge® MS C_{18} 2.5 μm, 10 × 50 mm). The compositions of **22–29** were confirmed by MALDI-TOF mass analysis. MALDI-TOF mass analysis. MALDI-TOF MS data ($[M-H]^-$) for **22–29**: **22**, found 3033.70 (calcd 3034.00); **23**, found 3090.36 (calcd 3089.03); **24**, found 3145.24 (calcd 3144.07); **25**, found 3048.53 (calcd 3048.02); **26**, found 3117.32 (calcd 3117.08); **27**, found 3187.85 (calcd 3186.25); **28**, found 3033.23 (calcd 3034.00); **29**, found 3048.78 (calcd 3048.02).

4.22. UV-melting experiments

UV-melting experiments were carried out using SHIMADZU UV-1650 and SHIMADZU UV-1800 spectrophotometers equipped with a T_m analysis accessory. Oligonucleotides and ssDNA or ssRNA were dissolved in 10 mM sodium phosphate buffer (pH 7.2) containing 100 mM NaCl to give a final concentration of each strand of 4 μM. The samples were annealed by heating at 100 °C followed by slow cooling to 15 °C. The melting profiles were recorded at 260 nm from 15 to 85 °C at a scan rate of 0.5 °C/min. The two-point average method was employed to obtain the T_m values and the final values were determined by averaging three independent measurements which were accurate to within 1 °C.

4.23. Enzymatic degradation experiments

Enzymatic degradation experiments were carried out under conditions of 1.75 μg/mL Crotalus admanteus venom phosphodiesterase (CAVP), 10 mM $MgCl_2$, 50 mM Tris–HCl (pH 8.0) and 7.5 μM each oligonucleotide at 37 °C. The amount of intact oligonucleotides was determined by reversed-phase HPLC (Waters XBridge® MS C_{18} 2.5 μm, 10 × 50 mm).

Acknowledgments

This work was supported in part by the Program for Promotion of Fundamental Studies in Health Sciences of the National Institute of Biomedical Innovation (NIBIO), the Program to Disseminate Tenure Tracking System of the Ministry of Education, Culture, Sports, Science and Technology, Japan (MEXT), and a Grant-in-Aid for Scientific Research on Innovative Areas (No. 22136006) from MEXT.

Supplementary data

Supplementary data associated with this article can be found, in the online version, at http://dx.doi.org/10.1016/j.bmc.2013.04.049.

References and notes

1. Reviews: Shukla, S.; Sumaria, C. S.; Pradeepkumar, P. I. *ChemMedChem* **2010**, *5*, 328; Obika, S.; Rahman, S. M. A.; Fujisaka, A.; Kawada, Y.; Baba, T.; Imanishi, T. *Heterocycles* **2010**, *81*, 1347; Yamamoto, T.; Narukawa, K.; Nakatani, M.; Obika, S. *Future Med. Chem.* **2011**, *3*, 339; (d) Prakash, T. P. *Chem. Biodiv.* **2011**, *8*, 1616; (e) Deleavey, G. F.; Damha, M. J. *Chem. Biol.* **2012**, *19*, 937.
2. Reviews: Crooke, S. T. *Annu. Rev. Med.* **2004**, *55*, 61; Gleave, M. E.; Monia, B. P. *Nat. Rev. Cancer* **2005**, *5*, 468; Chan, J. H.-P.; Lim, S.; Wong, W.-S. F. *Clin. Exp. Pharm. Phys.* **2006**, *33*, 533.
3. Obika, S.; Nanbu, D.; Hari, Y.; Morio, K.; In, Y.; Ishida, T.; Imanishi, T. *Tetrahedron Lett.* **1997**, *38*, 8735.
4. Nielsen, P.; Wengel, J. *Chem. Commun.* **1998**, 455.
5. Morita, K.; Hasegawa, C.; Kaneko, M.; Tsutsumi, S.; Sone, J.; Ishikawa, T.; Imanishi, T.; Koizumi, M. *Bioorg. Med. Chem. Lett.* **2002**, *12*, 73; Morita, K.; Takagi, M.; Hasegawa, C.; Kaneko, M.; Tsutsumi, S.; Sone, J.; Ishikawa, T.; Imanishi, T.; Koizumi, M. *Bioorg. Med. Chem.* **2003**, *11*, 2211.
6. Properties of 2′-amino-LNA and its six-membered analog, aza-ENA, were also reported by Wengel's group[9] and Chattopadhyaya's group,[10] respectively. However, there is no example in which they were compared.
7. Yahara, A.; Shrestha, A. R.; Yamamoto, T.; Hari, Y.; Osawa, T.; Yamaguchi, M.; Nishida, M.; Kodama, T.; Obika, S. *ChemBioChem* **2012**, *13*, 2513.
8. Shrestha, A. R.; Hari, Y.; Yahara, A.; Osawa, T.; Obika, S. *J. Org. Chem.* **2011**, *76*, 9891.
9. Singh, S. K.; Kumar, R.; Wengel, J. *J. Org. Chem.* **1998**, *63*, 10035.
10. Varghese, O. P.; Barman, J.; Pathmasiri, W.; Plashkevych, O.; Honcharenko, D.; Chattopadhyaya, J. *J. Am. Chem. Soc.* **2006**, *128*, 15173.

Nucleic Acid Modifications

DOI: 10.1002/anie.201300555

Selenomethylene Locked Nucleic Acid Enables Reversible Hybridization in Response to Redox Changes**

*Kunihiko Morihiro, Tetsuya Kodama, Kentefu, Yoshihiro Moai, Rakesh N. Veedu, and Satoshi Obika**

DNA and RNA play important roles not only for the storage and flow of genetic information but also for the modulation of gene expression within an organism. For example, non-coding RNAs regulate many biological processes such as cell proliferation, cell death, and cell development.[1–3] It has also been suggested that guanine-rich DNA sequences regulate a variety of gene expression through G-quadruplex structures.[4,5] Moreover, epigenetic DNA modifications, including 5-methylcytosine, have recently been reported to participate in various diseases.[6–8] These gene-regulation systems, which are said to be natural nucleic acid switches, are controlled by changes in biochemical environments and gene-expression levels within cells.

Recently, chemically modified nucleotides that can reversibly change their properties by sensing differences in the surrounding environment have attracted attention. Such artificial nucleotides show promise as nucleic acid switches regulated by biological functions, which are impossible for natural nucleic acid switches. Several external-stimulus-responsive nucleic acids have been developed by regulating hydrogen-bonding interactions between nucleobases,[9] stacking within the DNA helices,[10] or the inversion of helicity.[11] Herein, we designed and synthesized a new redox-responsive nucleotide focusing on the reversible oxidation/reduction of selenium, as well as incorporated it into an oligonucleotide (ON) and characterized its properties as a nucleic acid switch.

Locked nucleic acid (LNA)[12]/2′,4′-bridged nucleic acid (2′,4′-BNA)[13] **1** has a methylene bridge between the 2′-oxygen and 4′-carbon atoms of the ribose sugar, which locks it in the C3′-*endo* conformation (Figure 1a). ONs containing LNA show strong binding affinity against complementary DNA and RNA.[12,14] Since the initial synthesis, a number of

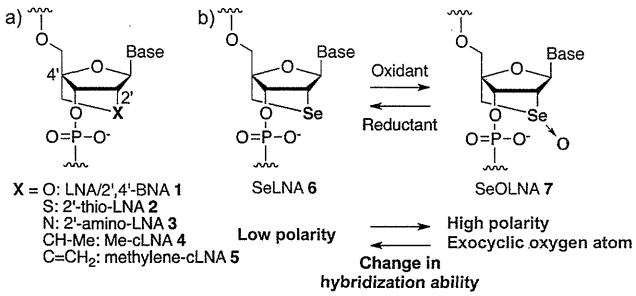

Figure 1. a) Formulas of 2′-substituted LNA analogues. b) Reversible structural change between SeLNA (**6**) and SeOLNA (**7**) by oxidant and reductant.

LNA analogues have been developed.[15] For example, 2′-thio-LNA (**2**)[16,17] and 2′-amino-LNA (**3**)[17,18] have the oxygen atom in the bridge replaced with sulfur and nitrogen atoms, respectively. These analogues show high binding affinity against complementary strands, similar to LNA, and we anticipated that the type of heteroatom at the 2′-position would have little influence on the binding properties of LNA analogues. On the other hand, it is known that the substituent on the bridged structure influences the hybridization property of LNA analogues because it interacts electrostatically and sterically with the minor groove of the duplexes. For example, Chattopadhyaya and co-workers reported that Me-cLNA (**4**), where the 2′-oxygen atom of LNA was replaced with a methyl-substituted carbon atom, shows reduced binding affinity for complementary RNA relative to LNA,[19] while Seth et al. reported that the replacement of the 2′-oxygen atom in LNA with an exocyclic methylene group does not affect the hybridization ability of modified ON [methylene-cLNA (**5**)].[20] These substituents in LNA analogues are located in the minor groove and thus can influence the duplex stability depending on their polarity and orientation.

Given this background, we designed a new LNA analogue possessing a low polaraity selenium atom at the 2′-position [SeLNA (**6**), Figure 1b]. Micura and co-workers reported the reversible oxidation/reduction of 2′-methylselenoguanosine in RNA;[21] therefore, a reversible structural change between SeLNA and its selenoxide-bridged analogue SeOLNA (**7**) should be possible. SeOLNA would have a highly polar selenoxide group in the bridge and the exocyclic oxygen atom

[*] K. Morihiro,[+] Kentefu, Prof. Dr. S. Obika
Graduate School of Pharmaceutical Sciences,
Osaka University
1-6 Yamadaoka, Suita 565-0871 (Japan)
E-mail: obika@phs.osaka-u.ac.jp
Prof. Dr. T. Kodama,[+] Y. Moai
Graduate School of Pharmaceutical Sciences,
Nagoya University (Japan)
Prof. Dr. R. N. Veedu
School of Chemistry and Molecular Biosciences,
The University of Queensland (Australia)
[+] These authors contributed equally to this work.

[**] This work was supported by the Japan Society for the Promotion of Science (JSPS), the Ministry of Education, Culture, Sports, Science and Technology (MEXT), and the Advanced Research for Medical Products Mining Programme of the National Institute of Biomedical Innovation (NIBIO). K.M. is grateful for a Research Fellowship for Young Scientists from JSPS.

Supporting information for this article is available on the WWW under http://dx.doi.org/10.1002/anie.201300555.

would be located in the minor groove of the duplex, hence the hybridization ability of SeOLNA is expected to be strikingly different from that of SeLNA.

The synthesis of SeLNA phosporamidite is summarized in Scheme 1. An arabino nucleoside derivative **8**[22] was converted into the triflate, which was treated immediately with sodium selenide[23] in EtOH/tetrahydrofuran (THF) to afford

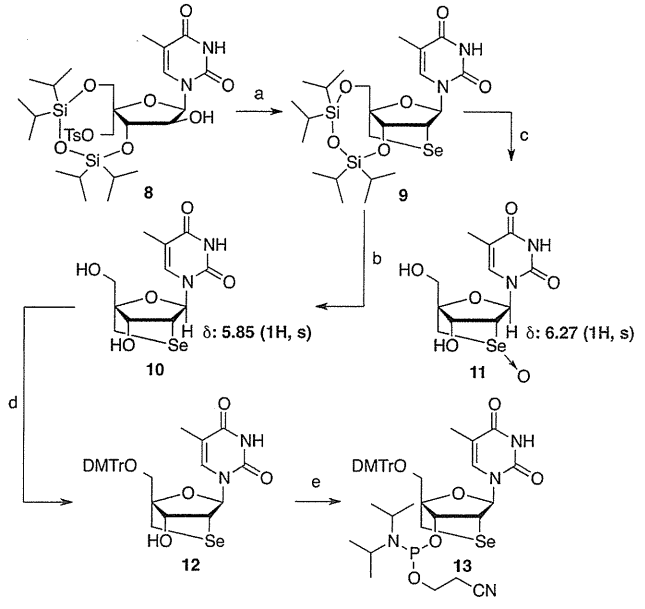

Scheme 1. Synthesis of SeLNA phosphoramidite **13**: a) 1) Tf_2O, pyridine, CH_2Cl_2, 0 °C to RT; 2) Se, $NaBH_4$, EtOH, THF, 60 °C, 44% yield (2 steps); b) TBAF, THF, 0 °C, 67% yield; c) 1) *m*CPBA, CH_2Cl_2, 0 °C; 2) TBAF, THF, 0 °C (2 steps); d) DMTrCl, pyridine, RT, 77% yield; e) 2-cyanoethyl-*N*,*N*-diisopropylchlorophosphoramidite, DIPEA, MeCN, RT, 82% yield. Tf = trifluoromethanesulfonyl, TBAF = tetra-*n*-butylammonium fluoride, DMTr = 4,4′-dimethoxytrityl, DIPEA = *N*,*N*-diisopropylethylamine.

the desired cyclized product **9**. Desilylation with tetra-*n*-butylammonium fluoride (TBAF) was carried out to give the corresponding nucleoside **10**. Alternatively, **9** was oxidized by *meta*-chloroperoxybenzoic acid (*m*CPBA) and converted into SeOLNA nucleoside **11** as a single diastereomer. The C3′-*endo* sugar conformation of **10** and **11** was confirmed by ^{1}H NMR spectroscopy where the H1′ signal was observed as a singlet.[24] We also examined the stereochemistry of the selenoxide group based on the change in the chemical shifts ($\Delta\delta$ values) induced by oxidation. Hartree–Fock (HF) and density functional theory (DFT) calculations of the (R_{Se})-isomer **S1** and (S_{Se})-isomer **S2** (see Supporting Information for formulas of **S1** and **S2**) clearly indicated that the experimental $\Delta\delta$ values of H1′, H6′α, and H6′β induced by oxidation were in very good agreement with the calculated ones for the (R_{Se})-isomer; therefore, we confirmed the stereochemistry of the selenium center of selenoxide **11** as the (R_{Se})-configuration (Supporting Information, Table S1). Tritylation at the primary hydroxy group of **10** with DMTrCl and phosphitylation at the secondary hydroxy group yielded phosphoramidite **13**. The amidite **13** was incorporated into ONs using conventional solid-phase phosphoramidite synthesis. The ON sequences used in this study are shown in Figure 2.

There have been reports of the oxidation of 2′-methylseleno RNA by iodine treatment during solid-phase synthesis;[21,25–28] however, we did not observe such oxidation of

```
14     5'-d(GCGTTTTTTGCT)-3'
15     5'-r(GCGUUUUUUGCU)-3'
16a-c  5'-d(GCGTTTTTTGCT)-3'
17a-c  5'-d(GCGTTTTTTGCT)-3'
18a-c  5'-d(GCGTTTTTTGCT)-3'
19a-c  5'-d(GCGTTTTTTGCT)-3'
20     5'-d(AGCAAAAAACGC)-3'
21     5'-r(AGCAAAAAACGC)-3'
MBa-b  5'-FAM-d(TTTTTTCTTTTGTCCCTTCTT-
                AAAAAA)-BHQ1-3'
```

Figure 2. ON sequences used in this study. Underlined bold characters indicate modified residues. Series **a** = SeLNA, **b** = SeOLNA, and **c** = LNA modifications in the ONs.

SeLNA-containing ONs. Moreover, SeLNA was found to be stable in air (Figure S3). This may be because SeLNA is stable against oxidants or that deoxygenation of SeOLNA occurs during DNA synthesis. Therefore, we investigated the redox properties of SeLNA in ONs. Initially, ON **16a** having one SeLNA unit was treated with hydrogen peroxide, and the resulting product was analyzed by reverse-phase (RP) HPLC at several reaction times (Figure 3a). The signal corresponding to ON **16a** completely disappeared within 12 hours and ON **16b** with SeOLNA was generated. Further oxidation to the selenone-bridged analogue was not observed in the MALDI-TOF mass spectra. We then reduced SeOLNA back to SeLNA using dithiothreitol (DTT) as a reducing agent; reduction of SeOLNA was complete within 12 hours. We also evaluated the concentration dependence of the redox reagents and confirmed that other redox systems could also

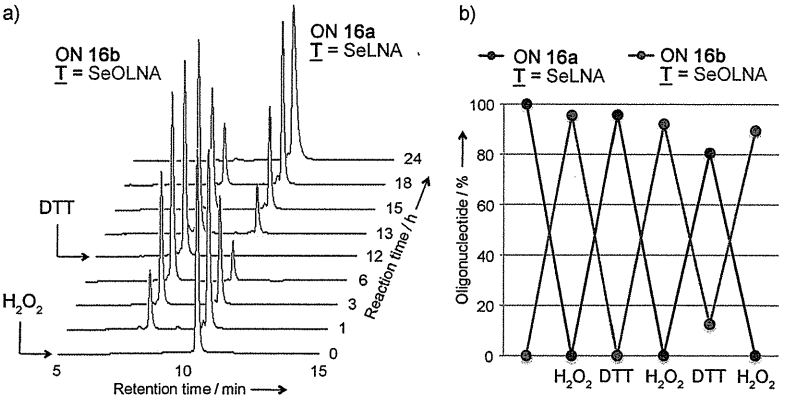

Figure 3. a) Reversible redox reaction of ON **16a** by H_2O_2/DTT observed by RP-HPLC. Conditions: ON **16a** (10 μM), sodium phosphate buffer (25 mM, pH 7.2), H_2O_2 (10 mM), DTT (10 mM), 37 °C. b) Repetitive redox reaction of ON **16a**. The percentages of ON **16a** and ON **16b** were obtained from the HPLC peak areas.

change the oxidation state of SeLNA (Figure S2). Moreover, redox reactions of ON **16a** using H_2O_2 and DTT were repeated, showing that the reaction was reversible at least five times in a row (Figure 3b). Thus, SeLNA has the potential to work as a redox switch for various biomolecules. There have been few reports on nucleosides or nucleotides that can reversibly change their structures and properties in response to the surrounding redox conditions.[29]

The hybridization ability of SeLNA- and SeOLNA-modified ONs to complementary DNA and RNA was evaluated by UV melting experiments and compared with LNA-modified ONs (Table 1). SeLNA- and SeOLNA-modified ONs formed more stable duplexes with an RNA complement than with a DNA complement, similar to other LNA analogues that were previously reported. As the number of modifications increased, the difference in hybridization ability between SeLNA and SeOLNA increased. Notably, ON **19a** with six consecutive SeLNA units showed a T_m value that was over 20°C higher than that of ON **19b** with six consecutive SeOLNA units (DNA: 71°C versus 44°C; RNA: 84°C versus 64°C). To clarify the factors affecting the differences in hybridization ability between SeLNA and SeOLNA, we studied the thermodynamic parameters by concentration-dependent melting experiments (Table 2; Tables S4,S5). Thermodynamic data indicated that the introduction of an SeLNA unit to an ON caused gains in entropy and losses in enthalpy compared to the natural duplexes. Especially, the high stability of duplexes formed between ON **19a** containing six consecutive SeLNAs and complementary DNA or RNA was due to the large entropy gain that more than compensated for the loss of enthalpy. On the other hand, duplex formation of ON **19b** with the complementary strand had a heavy disadvantage in terms of entropy. Egli, Rozners, and co-workers revealed that a 2′-fluoro-modified RNA duplex was dramatically dehydrated relative to an unmodified RNA duplex owing to the low hydrogen-bonding ability of the 2′-fluorine atom with water molecules.[30] Consecutive low-polarity selenium atoms in ON **19a** could contribute to partial dehydration of the minor groove during the transition from single strands to duplexes, resulting in a decrease in entropy loss as compared to SeOLNA and LNA. Additionally, decreased Watson–Crick H-bonding strength from the less electronegative 2′-selenium atom might lead to a disadvantage in terms of enthalpy.[31]

Table 1: Melting temperatures of SeLNA-, SeOLNA-, and LNA-modified duplexes.[a]

Duplex	T_m (ΔT_m per modification) [°C][b]		
T=	SeLNA	SeOLNA	LNA
16a–c/20	49 (−2.0)	46 (−5.0)	52 (+1.0)
17a–c/20	50 (−0.5)	43 (−4.0)	53 (+1.0)
18a–c/20	53 (+0.7)	44 (−2.3)	55 (+1.3)
19a–c/20	71 (+3.3)	44 (−1.2)	66 (+2.5)
16a–c/21	50 (+4.0)	48 (+2.0)	52 (+6.0)
17a–c/21	56 (+5.0)	50 (+2.0)	56 (+5.0)
18a–c/21	65 (+6.3)	56 (+3.3)	63 (+5.7)
19a–c/21	84 (+6.3)	64 (+3.0)	79 (+5.5)

[a] UV melting profiles were measured using a solution containing each oligonucleotide at a concentration of 4.0 μM in 100 mM NaCl and 10 mM sodium phosphate buffer at pH 7.2. [b] The T_m value given is the average of three independent measurements. ΔT_m values are calculated relative to the T_m values of unmodified DNA **14**/DNA **20** (51°C) or DNA **14**/RNA **21** (46°C) duplexes.

Table 2: Thermodynamic data for duplexes.[a]

Duplex	$\Delta H°$ [kcal mol^{-1}]	$\Delta S°$ [cal K^{-1} mol^{-1}]	$\Delta G°_{310K}$ [kcal mol^{-1}]
14/20	−84.6	−235	−11.6
19a/20	−65.2	−164	−14.5
19b/20	−96.0	−278	−9.9
19c/20	−80.3	−211	−15.0
14/21	−98.4	−282	−10.9
19a/21	−76.3	−187	−18.2
19b/21	−125.1	−346	−17.9
19c/21	−101.5	−262	−20.3

[a] These values were determined by van't Hoff plots with six data points (0.89–10.9 μM).

Interestingly, ON **19a** containing six consecutive SeLNA modifications showed much higher hybridization ability than ON **19c** containing six consecutive LNAs (DNA: 71°C versus 66°C; RNA: 84°C versus 79°C). Such excellent hybridization was also observed in ONs modified with six consecutive 2′,4′-BNA^{NC} modifications, which have a six-membered bridging structure.[22] Modeling studies suggest that the torsion angle (δ) and the maximum out-of-plane pucker (ν_{max}) of the SeLNA nucleoside was closer to that of 2′,4′-BNA^{NC} than that of LNA (Table S2). SeLNA has a five-membered bridge; however, the large selenium atom expands the size of the bridge and affects the hybridization properties.

Circular dichroism (CD) spectroscopy of SeLNA- and SeOLNA-modified duplexes were also performed to investigate their structural preferences (Figure S7). The spectrum of SeLNA-modified ON **19a** with complementary DNA **20** was very similar to that of a natural RNA/DNA (**15/20**) duplex. Moreover, minimal spectral differences were observed in the duplex formed between ON **19a** with RNA **21** compared with a natural RNA/RNA (**15/21**) duplex. These observations indicate that SeLNA formed duplexes with DNA and RNA in the same manner as natural RNA did. On the other hand, the CD spectra of SeOLNA-modified duplexes were different from that of natural DNA/DNA (**14/20**), DNA/RNA (**14/21**), RNA/DNA (**15/20**), and RNA/RNA (**15/21**) duplexes, suggesting that the duplexes modified with SeOLNA might not be typical A- and B-form duplexes, likely owing to local conformational alterations. However, it is possible that the CD spectra do not reflect the structure of SeOLNA-modified duplexes, because CD spectra may be affected by the existence of the UV-absorbing selenoxide group.

Measuring the T_m values revealed that there were great differences in hybridization ability between the SeLNA-modified ON and SeOLNA-modified ON when six consecutive modifications were introduced. This observation prompted us to use SeLNA in a nucleic acid switch to sense changes in the surrounding redox environment. We designed and synthesized a molecular-beacon-type DNA probe bearing

six consecutive SeLNA modifications in the stem region labeled with FAM at the 5′ end and BHQ1 at the 3′ end (Figure 4a, **MBa**).[32] We measured the change in the fluorescence intensity over time of **MBa** following addition of H_2O_2 (Figure 4b). The fluorescence intensity of **MBa** was gradually recovered in accordance with the reaction time, showing

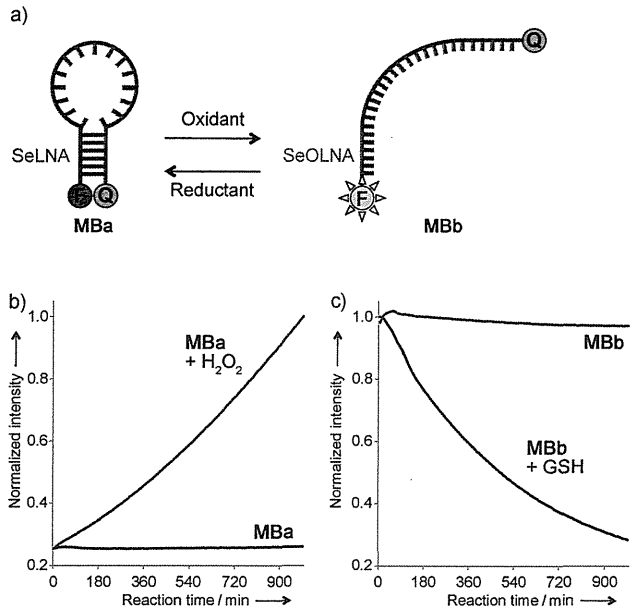

Figure 4. a) Scheme of the structure and fluorescent changes of an SeLNA-modified molecular-beacon-type probe (**MB**) in response to oxidant and reductant. b) Changes in the fluorescence intensity of **MBa** without (red) and **MBa** with (blue) H_2O_2. c) Changes in fluorescence intensity of **MBb** without (blue) and **MBa** with (red) GSH. Conditions: **MB** (0.1 μM), H_2O_2 or GSH (1000 μM), NaCl (100 mM), sodium phosphate buffer (10 mM, pH 7.2), 37°C.

dissociation of the hairpin structure. On the other hand, the addition of a reductant, glutathione (GSH), to the solution of **MBb** caused a decrease in the fluorescence intensity (Figure 4c). H_2O_2 is known as a marker for oxidative stress[33] and GSH as an important redox scavenger of reactive oxygen species.[34] Thus, **MB** could be used as a method for sensing the redox environment within a cell.

In conclusion, we synthesized a novel LNA analogue with a selenomethylene-bridged moiety, SeLNA. The selenium atom in the bridge of SeLNA could be converted into a selenoxide moity by treatment with an oxidant and reverted back to the selenide by treatment with a reductant. SeLNA-modified ONs showed high duplex-forming ability. Six consecutive SeLNA modifications imparted superior hybridizing ability compared to normal LNA modifications. This duplex-forming ability was disrupted by oxidation to SeOLNA. Finally, we demonstrated that a SeLNA-modified molecular-beacon-type probe could be used to sense changes in the surrounding redox environment. Recently, we reported the synthesis of SeLNA triphosphate and the enzymatic incorporation of an SeLNA nucleotide.[35] Further applications, such as the development of SeLNA-modified antisense agents targeting RNA overexpressed in oxidative environments and the evolution of SeLNA-modified aptamers towards the elucidation of aptamer structures by X-ray crystallography, are now in progress in our laboratory.

Received: January 22, 2013
Published online: April 11, 2013

Keywords: DNA hybridization · LNA · nucleic acids · redox chemistry · selenium

[1] L. He, G. J. Hannon, *Nat. Rev. Genet.* **2004**, *5*, 522–531.
[2] R. W. Carthew, *Curr. Opin. Genet. Dev.* **2006**, *16*, 203–208.
[3] R. Schickel, B. Boyerinas, S.-M. Park, M. E. Peter, *Oncogene* **2008**, *27*, 5959–5974.
[4] A. K. Todd, M. Johnston, S. Niedle, *Nucleic Acids Res.* **2005**, *33*, 2901–2907.
[5] J. L. Huppert, S. Balasubramanian, *Nucleic Acids Res.* **2005**, *33*, 2908–2916.
[6] P. A. Jones, D. Takai, *Science* **2001**, *293*, 1068–1070.
[7] G. Egger, G. Liang, A. Aparicio, P. A. Jones, *Nature* **2004**, *429*, 457–463.
[8] M. Hirst, M. A. Marra, *Int. J. Biochem. Cell Biol.* **2009**, *41*, 136–146.
[9] T. Ohmichi, Y. Kawamoto, P. Wu, D. Miyoshi, H. Karimata, N. Sugimoto, *Biochemistry* **2005**, *44*, 7125–7130.
[10] H. Asanuma, T. Ito, T. Yoshida, X. G. Liang, M. Komiyama, *Angew. Chem.* **1999**, *111*, 2547–2549; *Angew. Chem. Int. Ed.* **1999**, *38*, 2393–2395.
[11] R. Tashiro, H. Sugiyama, *Angew. Chem.* **2003**, *115*, 6200–6202; *Angew. Chem. Int. Ed.* **2003**, *42*, 6018–6020.
[12] S. K. Singh, P. Nielsen, A. A. Koshkin, J. Wengel, *Chem. Commun.* **1998**, 455–456.
[13] S. Obika, D. Nanbu, Y. Hari, K. Morio, Y. In, T. Ishida, T. Imanishi, *Tetrahedron Lett.* **1997**, *38*, 8735–8738.
[14] S. Obika, D. Nanbu, Y. Hari, J. Andoh, K. Morio, T. Doi, T. Imanishi, *Tetrahedron Lett.* **1998**, *39*, 5401–5404.
[15] S. Obika, S. M. A. Rahman, A. Fujisaka, Y. Kawada, T. Baba, T. Imanishi, *Heterocycles* **2010**, *81*, 1347–1392.
[16] R. Kumar, S. K. Singh, A. A. Koshkin, V. K. Rajwanshi, M. Meldgaad, J. Wengel, *Bioorg. Med. Chem. Lett.* **1998**, *8*, 2219–2222.
[17] S. K. Singh, R. Kumer, J. Wengel, *J. Org. Chem.* **1998**, *63*, 6078–6079.
[18] S. K. Singh, R. Kumer, J. Wengel, *J. Org. Chem.* **1998**, *63*, 10035–10039.
[19] J. Xu, Y. Liu, C. Dupouy, J. Chattopadhyaya, *J. Org. Chem.* **2009**, *74*, 6534–6554.
[20] P. P. Seth, C. R. Allerson, A. Berdeja, A. Siwkowski, P. S. Pallan, H. Gaus, T. P. Prakesh, A. T. Watt, M. Egli, E. E. Swayze, *J. Am. Chem. Soc.* **2010**, *132*, 14942–14950.
[21] H. Moroder, C. Kreutz, K. Lang, A. Serganov, R. Micura, *J. Am. Chem. Soc.* **2006**, *128*, 9909–9918.
[22] S. M. A. Rahman, S. Seki, S. Obika, H. Yoshikawa, K. Miyashita, T. Imanishi, *J. Am. Chem. Soc.* **2008**, *130*, 4886–4896.
[23] H. Liu, B. M. Pinto, *J. Org. Chem.* **2005**, *70*, 753–755.
[24] C. Altona, M. Sundaralingam, *J. Am. Chem. Soc.* **1973**, *95*, 2333–2344.
[25] C. Höbartner, R. Micura, *J. Am. Chem. Soc.* **2004**, *126*, 1141–1149.
[26] C. Höbartner, R. Rieder, C. Kreutz, B. Puffer, K. Lang, A. Polonskaia, A. Serganov, R. Micura, *J. Am. Chem. Soc.* **2005**, *127*, 12035–12045.
[27] B. Puffer, H. Moroder, M. Aigner, R. Micura, *Nucleic Acids Res.* **2008**, *36*, 970–983.

[28] J. Salon, J. Sheng, J. Gan, Z. Huang, *J. Org. Chem.* **2010**, *75*, 637–641.
[29] T. Baba, T. Kodama, K. Mori, T. Imanishi, S. Obika, *Chem. Commun.* **2010**, *46*, 8058–8060.
[30] P. S. Pallan, E. M. Greene, P. A. Jicman, R. K. Pandey, M. Manoharan, E. Rozners, M. Egli, *Nucleic Acids Res.* **2011**, *39*, 3482–3495.
[31] A. Patra, M. Paolillo, K. Charisse, M. Manoharan, E. Rozners, M. Egli, *Angew. Chem.* **2012**, *124*, 12033–12036; *Angew. Chem. Int. Ed.* **2012**, *51*, 11863–11866.
[32] S. Tyagi, F. R. Kramer, *Nat. Biotechnol.* **1996**, *14*, 303–308.
[33] D. Banerjee, U. K. Madhusoodanan, S. Nayak, J. Jacob, *J. Clin. Chim. Acta* **2003**, *334*, 205–209.
[34] M. E. Rice, *Neuroscientist* **2011**, *17*, 389–406.
[35] M. Wheeler, A. Chardon, A. Goubet, K. Morihiro, S. Y. Tsan, S. L. Edwards, T. Kodama, S. Obika, R. N. Veedu, *Chem. Commun.* **2012**, *48*, 11020–11022.

Neuroscience 263 (2014) 148–158

EFFECTS OF INTRAVENOUS ADMINISTRATION OF UMBILICAL CORD BLOOD CD34$^+$ CELLS IN A MOUSE MODEL OF NEONATAL STROKE

M. TSUJI,[a*] A. TAGUCHI,[a,c] M. OHSHIMA,[a] Y. KASAHARA,[c] Y. SATO,[d] H. TSUDA,[a] K. OTANI,[a] K. YAMAHARA,[a] M. IHARA,[a,b] M. HARADA-SHIBA,[a] T. IKEDA[e] AND T. MATSUYAMA[f]

[a] *Department of Regenerative Medicine and Tissue Engineering, National Cerebral and Cardiovascular Center Research Institute, 5-7-1, Fujishiro-dai, Suita, Osaka 565-8565, Japan*

[b] *Department of Neurology, National Cerebral and Cardiovascular Center Research Institute, 5-7-1, Fujishiro-dai, Suita, Osaka 565-8565, Japan*

[c] *Department of Regenerative Medicine Research, Institute of Biomedical Research and Innovation, 2-2, Minami-machi, Minatojima, Chuo-ku, Kobe 650-0047, Japan*

[d] *Division of Neonatology, Center for Maternal-Neonatal Care, Nagoya University Hospital, 65 Tsurumai-cho, Showa-ku, Nagoya 466-8560, Japan*

[e] *Department of Obstetrics and Gynecology, Mie University School of Medicine, 2-174, Edobashi, Tsu, Mie 514-8507, Japan*

[f] *Laboratory of Neurogenesis and CNS Repair, Institute for Advanced Medical Science, Hyogo College of Medicine, 1-1, Mukogawacho, Nishinomiya, Hyogo 663-8501, Japan*

Abstract—Neonatal stroke occurs in approximately 1/4000 live births and results in life-long neurological impairments: e.g., cerebral palsy. Currently, there is no evidence-based specific treatment for neonates with stroke. Several studies have reported the benefits of umbilical cord blood (UCB) cell treatment in rodent models of neonatal brain injury. However, all of the studies examined the effects of administering either the UCB mononuclear cell fraction or UCB-derived mesenchymal stem cells in neonatal rat models. The objective of this study was to examine the effects of human UCB CD34$^+$ cells (hematopoietic stem cell/endothelial progenitor cells) in a mouse model of neonatal stroke, which we recently developed. On postnatal day 12, immunocompromized (SCID) mice underwent permanent occlusion of the left middle cerebral artery (MCAO). Forty-eight hours after MCAO, human UCB CD34$^+$ cells (1×10^5 cells) were injected intravenously into the mice. The area in which cerebral blood flow (CBF) was maintained was temporarily larger in the cell-treated group than in the phosphate-buffered saline (PBS)-treated group at 24 h after treatment. With cell treatment, the percent loss of ipsilateral hemispheric volume was significantly ameliorated (21.5 ± 1.9%) compared with the PBS group (25.6 ± 5.1%) when assessed at 7 weeks after MCAO. The cell-treated group did not exhibit significant differences from the PBS group in either rotarod (238 ± 46 s in the sham-surgery group, 175 ± 49 s in the PBS group, 203 ± 54 s in the cell-treated group) or open-field tests. The intravenous administration of human UCB CD34$^+$ cells modestly reduced histological ischemic brain damage after neonatal stroke in mice, with a transient augmentation of CBF in the peri-infarct area.

Key words: neonatal stroke, neonatal encephalopathy, brain injury, umbilical cord blood, CD34$^+$ cell, cell-based therapy.

INTRODUCTION

Perinatal/neonatal stroke occurs in 1/2800 to 1/5000 live births and results in life-long neurological impairments: e.g., cerebral palsy, mental retardation, and epilepsy (Nelson and Lynch, 2004; Chabrier et al., 2011). The current treatment for infants with stroke is predominantly supportive, as there is no evidence-based specific treatment available (Roach et al., 2008; Chabrier et al., 2011). The onset of neonatal stroke is antenatal in some cases and is unknown in others. Hence, treatments that have a narrow therapeutic window, such as tissue plasminogen activator, are not feasible for perinatal/neonatal stroke. Cell-based therapy has attracted much attention as a novel treatment for a number of neurological diseases, including neonatal encephalopathy (NE) (Bennet et al., 2012), which encompasses stroke and hypoxic–ischemic encephalopathy (HIE) (Dammann et al., 2011). Apart from its possible regenerative properties, its wide therapeutic time window, up to days after the insult (Yasuhara et al., 2010; Donega et al., 2013), is one of the most attractive features of this therapy. This is astonishing considering the fact that almost all candidate drugs examined in animal models exhibit neuroprotection only when administered before or within a few hours after the insult.

Human umbilical cord blood (hUCB) contains many stem cell types, i.e., hematopoietic stem cells, endothelial progenitor cells, and mesenchymal stem cells (MSCs) (Ingram et al., 2004; Lee et al., 2004). CD34 is widely used as a marker of hematopoietic stem

*Corresponding author. Tel: +81-6-6833-5012; fax: +81-6-6835-5496.
E-mail addresses: tsuji.masahiro.ri@ncvc.go.jp (M. Tsuji), taguchi@fbri.org (A. Taguchi), oshima.makiko.ri@ncvc.go.jp (M. Ohshima), t-ikeda@clin.medic.mie-u.ac.jp (T. Ikeda), tomohiro@hyo-med.ac.jp (T. Matsuyama).

Abbreviations: ANOVA, analysis of variance; CBF, cerebral blood flow; GDNF, glial cell line-derived neurotrophic factor; HIE, hypoxic–ischemic encephalopathy; hUCB, human umbilical cord blood; HuNu, anti-human nuclei antibody; MCAO, middle cerebral artery occlusion; MNC, mononuclear cell; MSC, mesenchymal stem cell; NE, neonatal encephalopathy; PBS, phosphate-buffered saline; ROI, region of interest; SCID, severe combined immunodeficiency; UCBC, umbilical cord blood cell; VEGF, vascular endothelial growth factor.

0306-4522/13 $36.00
http://dx.doi.org/10.1016/j.neuroscience.2014.01.018

and endothelial progenitor cells (Rafii and Lyden, 2003). hUCB contains 10-times more $CD34^+$ mononuclear cells (MNCs) than does adult peripheral blood (Murohara et al., 2000). The proportion of $CD34^+$ cells in hUCB ranges from 0.3% (Sun et al., 2010) to 2.4% (de Paula et al., 2012), which is comparable to bone marrow (Cox et al., 2011). Because of this feature, hUCB has been used for hematopoietic stem cell transplantation in patients with hematological diseases and inherited metabolic disorders/neurodegenerative diseases, i.e., Hurler's syndrome, adrenoleukodystrophy, and Krabbe disease (Prasad et al., 2008). Apart from their hematopoietic properties, hUCB cells (hUCBCs) have myriad effects. Human $CD34^+$ cells secrete numerous cytokines, chemokines, and growth factors, including vascular endothelial growth factor (VEGF) (Majka et al., 2001). $CD34^+$ cells are less prevalent in the neonatal peripheral blood immediately after birth than in UCB and tend to decrease within the first 48 h after delivery (Kim et al., 2007). The basic concept underlying the intravenous administration of autologous UCBCs for NE is to replenish the reduced stem cells in systemic circulation, which may contribute to neuroprotection and/or enhance cerebral plasticity.

There are several dozen reports in the literature that have examined the effects of cell therapies in animal models of NE. Several cell types have been investigated (Chicha et al., 2014), including neural stem cells (Comi et al., 2008; Sato et al., 2008), MSCs (van Velthoven et al., 2010), multipotent adult progenitor cells (Yasuhara et al., 2006), and dental pulp-derived stem cells (Yamagata et al., 2013). Several cell sources have been investigated as well, i.e., rodent embryo (Comi et al., 2008; Sato et al., 2008), rodent or human bone marrow (Yasuhara et al., 2006; van Velthoven et al., 2010), and hUCB (Meier et al., 2006). Furthermore, several administration routes have also been investigated, i.e., intracerebral (Xia et al., 2010), intraperitoneal (Meier et al., 2006), and intranasal delivery (van Velthoven et al., 2013). Many studies have shown the benefits of cell therapy. Among these different cell therapies, the intravenous administration of autologous UCB treatment may have the lowest risk for clinical use in NE (Bennet et al., 2012). A few clinical trials using an intravenous administration of autologous UCB for NE are currently in progress (http://www.clinicaltrials.gov/, NCT00593242, NCT01506258, NCT01649648). However, little is known about the optimal protocol and the mechanisms of action of UCBC treatment. To date, there have been 15 reports in the literature examining the effects of UCBC treatment in rodent models of NE. These studies used either whole of the MNC fraction (Meier et al., 2006; de Paula et al., 2009, 2012; Pimentel-Coelho et al., 2010; Rosenkranz et al., 2010, 2012, 2013; Yasuhara et al., 2010; Geißler et al., 2011; Bae et al., 2012; Dalous et al., 2012; Wasielewski et al., 2012; Wang et al., 2013) or MSCs derived from hUCB (Xia et al., 2010; Kim et al., 2012). The effects of other cell populations in UCB for NE remain unknown. In this study, we focused on the $CD34^+$ cell fraction of hUCB. We have previously reported the beneficial effects of the systemic administration of hUCB-$CD34^+$ cells in an adult mouse model of stroke (Taguchi et al., 2004a). The objective of this study was to examine the effects of the intravenous administration of hUCB-$CD34^+$ cells on post-stroke recovery in a mouse model of neonatal stroke.

EXPERIMENTAL PROCEDURES

Animals and surgery

All experiments were performed in accordance with the NIH Guide for the Care and Use of Laboratory Animals and were approved by the Experimental Animal Care and Use Committee of the National Cerebral and Cardiovascular Center.

Ninety-one postnatal day 12 (P12) male and female mouse pups with severe combined immunodeficiency (SCID) (CB-17/Icr-scid/scidJcl; CLEA Japan Inc., Tokyo, Japan) were prepared for the experiments. P8–12 mice are considered comparable to human full-term (P0) neonates with regard to brain maturation (Hagberg et al., 2002); some authors argue that P12 mice are more representative of human full-term neonates (Charriaut-Marlangue et al., 2013). The novel model of neonatal stroke that we recently reported (Tsuji et al., 2013) uses CB-17 (CB-17/Icr-+/+Jcl) mouse pups, which are immunocompetent. As human cells were administered to mice, in the present study, we used immunocompromized animals to minimize immunological reactions due to xenotransplantation. The SCID mice used in the present study were derived from the same strain with the same genetic background as CB-17 mice. All efforts were made to minimize the number of animals used and their suffering.

Permanent middle cerebral artery occlusion (MCAO) was produced according to previously reported methods (Tsuji et al., 2013). Under isoflurane anesthesia (4.0% for induction and 1.5–2.0% for maintenance), a hole was made in the left temporal bone. The left middle cerebral artery (MCA) was electrocauterized and disconnected distal to crossing the olfactory tract. Thirteen pups underwent open-skull surgery without MCA electrocoagulation and served as sham-surgery controls. Five pups were excluded from the experimental analysis owing to bleeding during surgery. All analyses were performed by investigators who were blinded to the experimental group.

Cerebral blood flow (CBF) measurements

The cortical surface CBF was measured by a laser speckle flowmetry imaging system (Omegazone, Omegawave Inc., Tokyo, Japan) 24 h after MCAO, 24 h after treatment (i.e., 72 h after MCAO), and 1 and 7 weeks after treatment, as described previously, with one minor modification (Ohshima et al., 2012). We measured the CBF in two regions of interest (ROIs) through the intact skull with an open-scalp: the Core (the ischemic core region of the MCA territory) and the MCA region (the broader region covering most of the MCA territory, including the Core). The same grid was

used to set the two matching regions on the contralateral side. To analyze the influence of the treatment on the CBF in the peri-infarct regions, we measured the area in which the CBF was not attenuated, which we defined as the "well-perfused area." By observing the contralateral CBF visually, the area in which the CBF appeared equal to the corresponding contralateral side was manually demarcated using NIH Image software (ImageJ, 1.43r, NIH, Bethesda, MD, USA). For analytical accuracy of ROIs between animals and serial imaging, we set the ROI based on a line drawn from bregma to lambda, rather than basing it on the actual MCA-perfused territory. The percent of the well-perfused area was calculated by the ratio of the well-perfused area out of an area of a square grid, which primarily covered the MCA-perfused territory (Fig. 1A). All pups exhibited CBF reduction in the MCA territory after the MCAO. However, three mice exhibiting a mild CBF reduction, which was defined as a CBF ratio (ipsilateral/contralateral MCA region) > 0.80 at 24 h after MCAO, were removed from the study.

Administration of hUCB-CD34$^+$ cells after stroke

Seventy mice with MCAO were randomly assigned to one of two groups that received hUCB-CD34$^+$ cells (UCBC group) or phosphate-buffered saline (PBS group). Human UCB-CD34$^+$ cells were purchased from Lonza Inc. (Walkersville, MD, USA). The purity was >95%, and the viability of the cells was >95%. Forty-eight hours after the stroke, a skin incision was made under isoflurane anesthesia, and the left femoral vein was exposed. hUCB-CD34$^+$ cells (1×10^5 cells), or the same volume (40 μl) of PBS, were carefully infused into the femoral vein over 3 min using a 35G needle. We selected the dose of 1×10^5 hUCB-CD34$^+$ cells in the present study as the dose of 5×10^5 cells was beneficial in our previous study in an adult mouse model (Taguchi et al., 2004a). We selected the timing of cell administration at 48 h after the insult on the basis of our previous studies (Taguchi et al., 2004a; Uemura et al., 2012).

Behavioral tests

Rotarod and open-field tests were performed as described previously (Tsuji et al., 2013). Sensorimotor skills were evaluated 9 days and 7 weeks after the insult in the rotarod test. The rotarod accelerated from 4 to 40 rpm over 5 min (Muromachi Kikai Co., Ltd., Tokyo, Japan). The time until the mouse fell off the rotating drum was recorded for five consecutive sessions, and the average time spent on the drum was used for statistical comparison.

Locomotor and exploratory behaviors were evaluated 5 and 7 weeks after the insult using the open-field test.

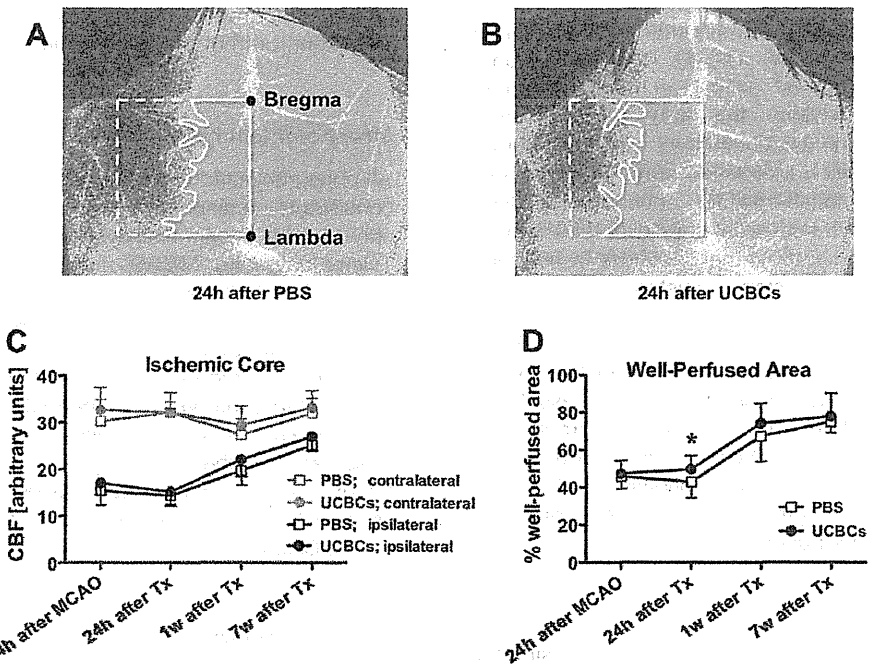

Fig. 1. Cerebral blood flow. (A, B) Representative images of the cerebral blood flow (CBF) 24 h after treatment (i.e., 72 h after the middle cerebral artery occlusion (MCAO)). The CBF was decreased in the MCA region on the ipsilateral side, which is indicated by the bluish color, after the MCAO insult. (C) There were no significant differences between the PBS-treated and human umbilical cord blood CD34$^+$ cell (UCBC)-treated groups with regard to CBF in the ischemic core. (D) However, with regard to the area of CBF reduction, there was a significant difference in the ratio of the area in which CBF was maintained (the area delineated by white lines in A, B) out of an area of a square (the square delineated by white dotted lines). The square was set based on a line drawn from bregma to lambda. We defined the ratio as the "% well-perfused area." Differences between groups were tested using a two-way repeated measures ANOVA. A post hoc test showed that the% well-perfused area was significantly larger in the UCBC group compared with the PBS group at 24 h after the treatment. *$P < 0.05$ (PBS-treated group $n = 10$–12 at each time point, except at 7 weeks after treatment ($n = 5$); UCBC-treated group $n = 11$–13 at each time point, except at 7 weeks after treatment ($n = 4$)). Tx; treatment.

Animals were allowed to search freely in a box (30 × 30 cm) for 30 min in a light environment and for the subsequent 30 min in a dark environment (Taiyo Electric Co., Ltd., Osaka, Japan). Infrared beams were mounted at specific intervals on the X-, Y-, and Z-banks of the open-field. The total number of beam crossings by the animal was counted and scored as "locomotion" for the horizontal movement and as "rearing" for the vertical movement.

Histological analyses

A morphological evaluation of the brain injury was performed as described previously (Tsuji et al., 2012, 2013). Animals were perfusion-fixed intracardially with 4% paraformaldehyde at 12 days or 7 weeks after the insult. The brain was removed and sectioned coronally in 1-mm-thick slices. The areas of the ipsilateral and contralateral hemispheres in each brain section were measured using ImageJ. The hemispheric volume was estimated by integrating the hemispheric areas. The % stroke volume was calculated as follows: ((contralateral volume – viable ipsilateral volume)/contralateral volume) × 100%. This model causes a pure cortical stroke with mild secondary injury in the thalamus and the corpus callosum, and the hemispheric volume effectively represents the histological injury (Tsuji et al., 2013).

Immunohistochemistry

Coronally sectioned brain slices were covered in tissue freezing medium (O.C.T. Compound, Sakura Finetek USA Inc., Torrance, CA, USA). Coronal sections (10 μm) were prepared using a cryostat (Leica Biosystems Inc., Wetzler, Germany). Sections were subjected to immunohistochemistry with anti-human nuclei antibody (HuNu) (Merck Millipore, Billerica, MA, USA, 1:30) and mouse-specific antibody to CD31 antigen expressed by endothelial cells (BD Biosciences, San Jose, CA, USA, 1:100); the secondary antibodies included anti-mouse Envision+ system-HRP Labeled Polymer and biotinylated anti-rat immunoglobulin (Dako Cytomation, Glostrup, Denmark), respectively. Nuclei were stained with hematoxylin after the HuNu staining. When analyzing the CD31-positive blood vessel, we defined the "peri-infarct area" as the external (non-ischemic) regions within 200 μm of the border of the post-stroke area, as described previously (Nakano-Doi et al., 2010). The lengths and diameters of blood vessels were measured using ImageJ.

Statistics

The mortality rate of the animals was analyzed using the Fisher's exact test. Differences in body weight were assessed using a one-way analysis of variance (ANOVA), followed by the Bonferroni test. The percent volume loss was assessed using a Student *t*-test. CBF, rotarod and open-field test outcomes were assessed using a two-way repeated measures ANOVA, followed by the Bonferroni test. Parameters in blood vessels were assessed using a two-way ANOVA, followed by the Bonferroni test. Differences were considered significant at $P < 0.05$. The results are expressed as the mean ± standard deviation (SD), unless otherwise noted.

RESULTS

Mortality and body weight

Mortality rates did not differ between the PBS and UCBC groups: 1 out of 35 mice in the PBS group and 2 out of 35 mice in the UCBC group. Body weights at the time of surgery (P12), and at 7 days (P21) and 7 weeks after the treatment (P63), did not differ among the three groups, including the sham-surgery control group (Table 1).

CBF

With regard to the degree of CBF reduction, there were no significant differences between the PBS and UCBC groups, either in the ischemic core (Fig. 1A–C) or in the MCA region (data not shown). However, with regard to the area of CBF reduction, a two-way repeated measures ANOVA showed that there was a significant group difference in the % well-perfused area: i.e., the areas where CBF was maintained were different (Fig. 1A, B, and D). A post hoc test showed that the % well-perfused area was significantly larger in the UCBC group compared with the PBS group at 24 h after the treatment, but not at the other time points measured.

Morphological brain injury

All pups subjected to MCAO exhibited cortical infarct and consistent hemispheric volume loss when assessed either 12 days or 7 weeks after the insult (Fig. 2A, B). Twelve days after MCAO, the mean % stroke volume did not differ between the PBS and UCBC groups, 20.7 ± 3.3% and 21.3 ± 2.4%, respectively (Fig. 2A). Seven weeks after MCAO, the mean% stroke volume in the UCBC group (21.5 ± 1.9%) was significantly ameliorated compared with the PBS group (25.6 ± 5.1%) (Fig. 2B–D). No sex differences in % stroke volume were observed in either of the groups (male 26.2 ± 3.9 vs. female 24.8 ± 6.5% in the PBS group, male 21.4 ± 1.2 vs. female 21.5 ± 2.3% in the UCBC group, at 7 weeks after MCAO).

Table 1. Body weights

	P12	P21	P63
Sham-surgery	6.9 ± 0.6	8.6 ± 0.5	20.0 ± 1.7
MCAO + PBS	6.7 ± 0.7	8.0 ± 0.7	18.2 ± 3.6
MCAO + UCBCs	6.7 ± 0.7	7.9 ± 0.7	18.2 ± 3.1

Body weights (g) (mean ± SD) at postnatal day 12 (P12, the day of surgery), P21 (7 days after the treatment), and P63 (7 weeks after the treatment) were not different between groups. MCAO, middle cerebral artery occlusion; PBS, phosphate-buffered saline; UCBCs, human umbilical cord blood $CD34^+$ cells.

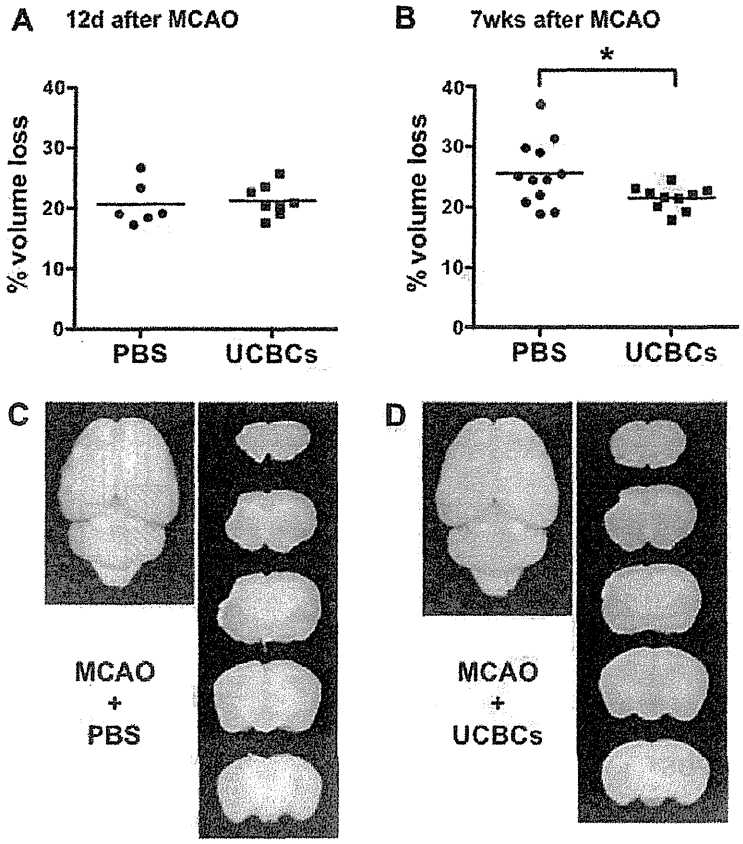

Fig. 2. Morphological brain injury. (A) Twelve days after middle cerebral artery occlusion (MCAO), the mean % stroke volume did not differ between the PBS-treated and human umbilical cord blood CD34$^+$ cell (UCBC)-treated groups. (B) Seven weeks after MCAO, the mean % stroke volume in the UCBC group was significantly ameliorated compared with the PBS group. (C) Representative images of brains 7 weeks after MCAO. $^*P < 0.05$.

Localization of hUCB-CD34$^+$ cells

Very few donor cells stained with human antinuclear antibody were identified in the brain (a few stained cells per the entire coronal section) 24 h after the intravenous injection ($n = 5$), most of which were located around blood vessels (Fig. 3). The stained cells were hardly identified 10 days after the injection ($n = 5$) (data not shown).

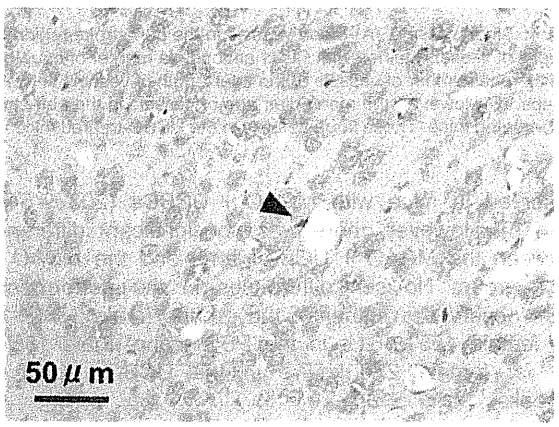

Fig. 3. Administered human umbilical cord blood CD34$^+$ cells. Very few donor cells, i.e., human umbilical cord blood CD34$^+$ cells stained with human antinuclear antibody, were identified in the brain 24 h after the intravenous injection. Donor cells that were identified were localized around blood vessels (arrowhead).

Blood vessels

We analyzed blood vessels in the region bordering the cortical infarct at 7 weeks after MCAO (Fig. 4A). There were no significant differences in either the number of vessels or the total length of vessels between the PBS and UCBC groups (Fig. 4B–E). However, the mean diameter of vessels was significantly larger in the UCBC-treated mice compared with the PBS-treated mice (Fig. 4B, C, and F). These large vessels in the UCBC-treated mice were observed only in the region bordering the cortical infarct and not in the other regions of the ipsilateral side or in the contralateral side.

Rotarod performance

Sensorimotor performance, as assessed by a rotarod treadmill at 9 days and 6 weeks after the insult, was analyzed by a two-way repeated measures ANOVA. There were significant group, but not time, differences. Compared with the performance in the sham-surgery group (238 ± 46 s, at 6 weeks), the performance was significantly impaired in mice with MCAO + PBS (175 ± 49 s), while no significant impairment was

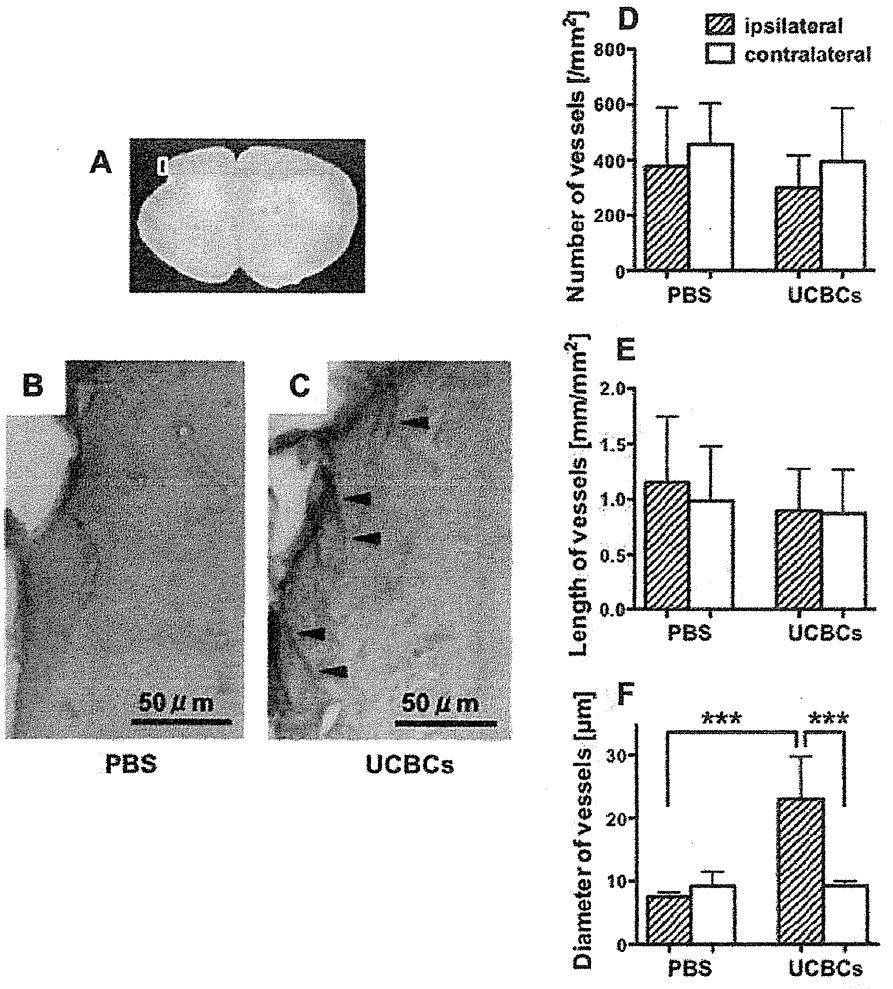

Fig. 4. Blood vessels. (A) Blood vessels in the peri-stroke region (small white square) were analyzed 7 weeks after MCAO. (B, C) Representative images of vessels stained with CD31 antibody (a marker of endothelial cells) in the peri-stroke regions. (D, E) There were no significant differences in either the number of vessels or the total length of vessels between the PBS-treated and human umbilical cord blood $CD34^+$ cell (UCBC)-treated groups. (F) However, the mean diameter of vessels in the peri-stroke region was significantly larger in the UCBC-treated mice compared with the PBS-treated mice. These large vessels in the UCBC-treated mice were only observed in the peri-stroke regions of the cortical infarct. $^{***}P < 0.001$.

observed in mice with MCAO + UCBCs (203 ± 54 s) (Fig. 5). However, there was no significant difference between the MCAO + UCBC group and the MCAO + PBS group. No sex differences in the performance were observed in either of the groups (male 188 ± 32 vs. female 155 ± 61 s in the PBS group, male 185 ± 43 vs. female 220 ± 57 s in the UCBC group, at 6 weeks).

Open-field activities

We initially analyzed the overall activities during 60-min sessions at 5 and 7 weeks after the insult using a two-way repeated measures ANOVA (data not shown). We then analyzed the temporal changes throughout a 60-min session in 5-min increments using a two-way repeated measures ANOVA (Fig. 6A, B). Compared with sham-surgery mice, mice with MCAO did not exhibit significant behavioral alterations in either locomotion or rearing at either time point; one exception

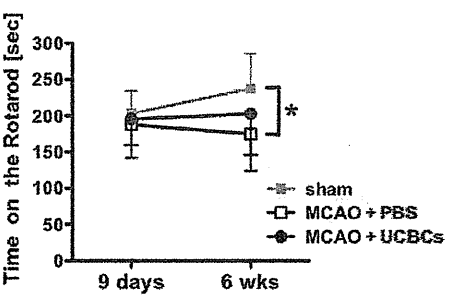

Fig. 5. Rotarod test. Repeated-measures two-way ANOVA showed significant group differences in sensorimotor performance. Performance was significantly impaired in mice with MCAO treated with PBS compared with sham-surgery mice. In contrast, performance was not impaired in mice with MCAO treated with human umbilical cord blood $CD34^+$ cells (UCBCs) compared with sham-surgery mice. However, there was no significant difference between the MCAO + UCBCs group and the MCAO + PBS group. $^*P < 0.05$. (sham $n = 10$; MCAO + PBS $n = 12$; MCAO + UCBCs $n = 16$, 9 days after the insult, i.e., 1 week after the treatment. $n = 10$ in each group, 6 weeks after the insult).

was mice with MCAO treated with either PBS or UCBCs that exhibited significantly less prominent responses to the dark environment with respect to locomotion at both 5 and 7 weeks after the insult. Overall, UCBC treatment did not significantly alter the behaviors in the mice with neonatal stroke, as assessed with the open-field test.

DISCUSSION

Only two cell types, the whole MNC fraction and MSCs, in hUCB have been investigated as cell therapies in animal models of NE to date. In the present study, the intravenous administration of hUCB-CD34$^+$ cells, which are mostly hematopoietic stem cells and endothelial progenitor cells, modestly ameliorated histological brain injury after neonatal stroke in mice. The effects were, at least in part, due to the improved CBF in the ischemic penumbra during the subacute phase of stroke, which may be associated with the increased mean diameter of blood vessels observed in the peri-infarct area during the chronic phase.

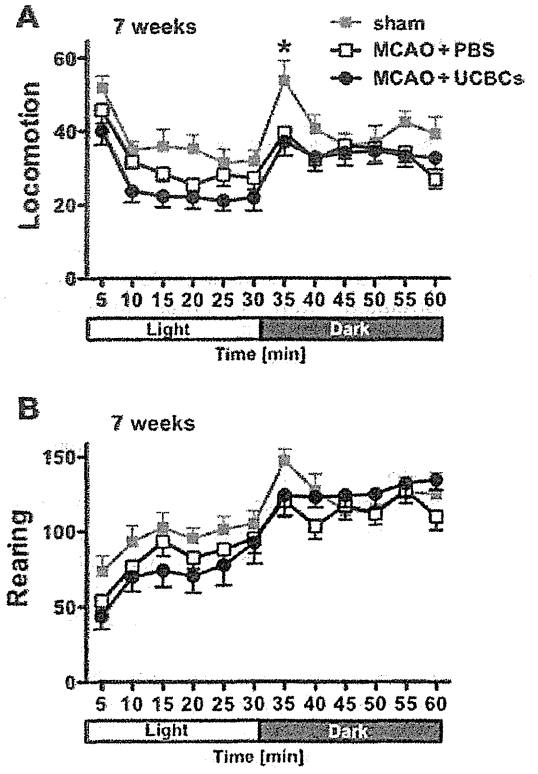

Fig. 6. Open-field test. Temporal changes in activities were analyzed in 5-min increments by a repeated-measures two-way ANOVA. (A) With respect to locomotion (horizontal movement), the mice in all three groups became hyperactive in response to the dark environment when assessed at 7 weeks after the insult. However, the response was significantly weaker in the mice with MCAO treated with either PBS or human umbilical cord blood CD34$^+$ cells (UCBCs) compared with the sham-surgery mice. (B) With respect to rearing (vertical movement), there were no significant group differences at 7 weeks after the insult. UCBC treatment did not significantly alter behavior in the mice with neonatal stroke. *$P < 0.05$ compared with the MCAO + PBS and MCAO + UCBCs groups. Mean ± SEM. (sham $n = 13$; MCAO + PBS $n = 17$; MCAO + UCBCs $n = 13$).

The purpose of the present study was to examine the potential of the CD34$^+$ cell fraction in human UCB; SCID mice, which are deficient in functional B and T lymphocytes because of a single gene mutation, were transfused with hUCB-CD34$^+$ cells. Hence, the present study used xenotransplantation; thus, caution should be exercised when translating the data obtained in the present study into the clinic. We used immunocompromized mice to minimize the undesirable immunological and inflammatory reactions caused by xenotransplantation as these reactions are not induced in autologous transfusion, which is the expected paradigm in the clinical application. To date, no study has examined the effects of allogeneic transplantation with UCBCs in rodent models of brain injury. One reason is because the rodent UCB is different from the human UCB; unlike in humans, mouse CD34$^+$ cells are not hematopoietic cells (Osawa et al., 1996). In addition, collecting rodent UCBCs is technically difficult.

We chose the timing of the cell transfusion to be 48 h after the brain injury for numerous reasons. The optimal time window of hUCBC therapies in animal models of NE has not been examined. UCBCs were administered 24 h after the brain injury in most NE studies (Table 2). Recent data on UCBCs and other types of stem cells in adult rodent models suggest that a later timing of transfusion, i.e., 48 or 72 h after the insult, is more beneficial (Newcomb et al., 2006; Rosenblum et al., 2012; Uemura et al., 2012).

One of the key features of this study is that it was performed using a highly reproducible model of NE, in which the locations of the infarct and peri-infarct areas were easily distinguishable and consistent between animals. During the first hours after brain injury, a detrimental biological cascade begins, and cells are destined to be damaged. We assumed that the neuroprotective effects would be limited when animals were treated 48 h after the insult, even if the cell treatment was potent. In fact, the hUCB-CD34$^+$ cell treatment achieved a modest, but statistically significant, amelioration of the brain injury. Similarly, the cell treatment exhibited a statistically significant augmentation of the CBF in the peri-infarct region, but not in other regions. These results suggest that the cell therapy exerts neuroprotective effects only in the peri-infarct area and not in the ischemic core. Moreover, these results suggest that it is crucial to examine the effects of treatment in a region-specific manner in a highly reproducible model.

The amelioration rate of cerebral tissue loss by the UCBC therapy was relatively small, and none of the UCBC-treated mice exhibited outstanding improvement; there may be a limit of the improvement in % stroke volume, e.g., 17.5% in this study. This implies that the ischemic core cannot be rescued or restored by cell treatment. The result is well conceivable as the model used in the present study is a permanent MCAO model in mice with a CB-17 strain background, which has little anastomoses between MCA and other cerebral arteries (Taguchi et al., 2010). Even after removing the pup with